UNIVERSITY OF TROMSØ UIT

FACULTY OF HEALTH SCIENCES
DEPARTMENT OF MEDICAL BIOLOGY

Structure and function of *Scaptodrosophila lebanonensis* alcohol dehydrogenase

Yimingjiang Wuxiuer

A dissertation for the degree of Philosophiae Doctor
July 2012

MSB
BioStruct

Yimingjiang Wuxiuer has been enrolled in BioStruct, the Norwegian national graduate school in Structural biology and in the PhD school in Molecular and Structural Biology at the University of Tromsø

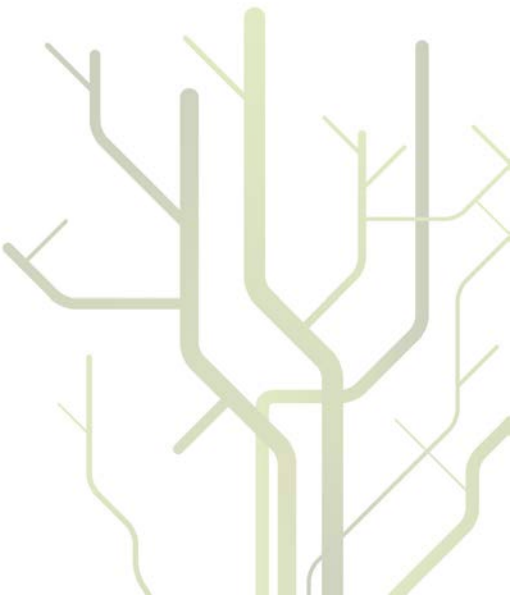

Structure and function of *Scaptodrosophila lebanonensis* alcohol dehydrogenase

Yimingjiang Wuxiuer

PhD Thesis
2012

Department of Medical Pharmacology and Toxicology
Institute of Medical Biology
Faculty of Health Sciences
University of Tromsø
Norway

Contents

ACKNOWLEDGEMENTS

This project was carried out at the University of Tromsø from 2008 – 2012. The work was supported by grants from the Norwegian Cancer Society and the University of Tromsø, and by CPU-hours from NOTUR - The Norwegian metacenter for computational science.

I would like to express my special thanks to my supervisors, Professor Ingebrigt Sylte and Professor Jan-Olof Winberg. This thesis would not have been possible without their help, support and patience. I would also like to thank Associate Professor Kurt Kristiansen and Senior Engineer Eli Berg who gave me the help in the lab. It is an honor for me to work together with our collaborators from different countries. I would especially like to thank Professor Neus Cols who gave me the full support to protect the enzyme sample from lab all the way to the airport at Barcelona. It was a wonderful, exciting and adventurous trip.

I would like to acknowledge the technical assistances from the Stallo and Schrodinger support teams with my work of molecular modelling on the super computer. My gratitude also goes to all the other members of the faculty, for their kindness, humour and creativity.

Tromsø, July 2012

Yimingjiang Wuxiuer

LIST OF PAPERS

3 papers are included in this thesis:

1. An intact eight-membered water chain in drosophilid alcohol dehydrogenases is Essential for Optimal Enzyme Activity

   FEBS journal, 2012, in press, DOI: 10.1111/j.1742-4658.2012.08675.x

2. Comparative molecular dynamic simulations of wild type and Thr114Val mutated *Scaptodrosophila lebanonensis* alcohol dehydrogenase

   Manuscript, 2012

3. QM/MM studies of the catalytic mechanism of short chain alcohol dehydrogenases

   Manuscript, 2012

ABBREVIATIONS

ADHs	Alcohol dehydrogenases enzymes
ADH^S	Slow alcohol dehydrogenase from *drosophilid* melanogaster
ADH^F	Fast alcohol dehydrogenase from *drosophilid* melanogaster
ADH^{UF}	Ultrafast alcohol dehydrogenase from *drosophilid* melanogaster
NAD(P)	Nicotinamide adenine dinucleotide (phosphate)
17-β-HSD1	17-β-hydroxysteroid dehydrogenase type 1
17-β-HSD2	17-β-hydroxysteroid dehydrogenase type 2
ABAD	Aβ-binding alcohol dehydrogenase
AD	Alzheimer's disease
AM1	Austin model 1
AMBER	Assisted Model Building with Energy Refinement
$_{app}K_i$	Apparent inhibition constant
Aβ	Amyloid-β
B3LYP	Becke, three-parameter, Lee-Yang-Parr functional
BPTI	Pancreatic trypsin inhibitor
CASPT2	Complete active space with second-order perturbation theory
CASSCF	Complete active space self-consistent field
CG	Conjugate gradient
CHARMM	Chemistry at Harvard macromolecular mechanic
CM	Chorismate mutase
CoA	Co-enzyme A
DADHs	*Drosophilid* alcohol dehydrogenases
DFT	Density function theory
D*m*ADH	*Drosophila melanogaster* alcohol dehydrogenases
$DmADH^S$	Slow alloenzymes from drosophila melanogaster
E1	Oestrone
E2	17-β-estradiol
EFP	Effective fragment potential
fs	Femtosecond
GROMOS	Acronym of the groningen molecular simulation
HF	Hartree-Fock
HSDs	Hydroxysteroid dehydrogenases enzymes
HTVS	high throughput virtual screening
ICM	Internal coordinate mechanics
k	Rate constant
K_{cat}	First-order rate constant
K_d	Dissociation constant
K_i	Inhibition constant

K_m	Michaelis-Menten constant
LDR	Long-chain dehydrogenase/reductases
MC	Monte carlo
MD	Molecular dynamic
MDR	Medium-chain dehydrogenase/reductases
MP	Møller-Plesset pertubation theory
M_r	Relative molecular mass
MRCI	Multi-reference ab initio methods
NMR	Nuclear magnetic resonance
NR	Newton-Raphson
ns	Nanosecond
OPLS-AA	All atom optimized potentials for liquid simulations
PDB	Protein data bank
PHBH	Para-hydroxybenzoate hydroxylase
PM3	Parametric method number 3
ps	Picosecond
QM/MM	Quantum mechanics and molecular mechanics
RMSD	Root-mean-square deviation
RMSF	Root-mean-square fluctuation
SAC-CI	Symmetry-adapted cluster−configuration interaction method
SCC-DFTB	Self-consistent charge density-functional tight binding method
SD	Steepest descent
SDR	Short-chain dehydrogenase/reductases
*Sl*ADH	*Scaptodrosophila lebanonensis* alcohol dehydrogenases
SP	Standard precision
TD-DFT	Time-dependent density function theory
UFF	Universal force field
XP	Extra precision
ΔG	Free energy of binding

1 Introduction

1.1 Alcohol dehydrogenases

Alcohol dehydrogenases (ADH) are a group of enzyme catalyzing the oxidation of alcohols to aldehydes and the reduction of aldehydes to alcohol by using nicotinamide adenine dinucleotide phosphate NAD(P)(H) as coenzyme [1]. Based on the length of primary sequence, they are classified into short-chain (SDR), medium-chain (MDR) and long-chain (LDR) dehydrogenase/reductases [2-5]. Through genome sequencing projects it is now clear that distinct families of ADH encode a large group of gene products within nearly every genome [6, 7]. This wide representation of oxidoreductases highlights their importance and functional diversity in the physiology of organisms reaching from prokaryotes to mammals [6]. ADHs from *drosophilid* species (*D*ADHs) are typical members of the SDR family.

1.2 Functions of short-chain dehydrogenases/reductases

SDRs form a large and evolutionary old family of enzymes, and currently more than 47000 members, including species variants are known [8]. SDR members catalyze diverse biochemical reactions such as isomerization, epimerization and oxidoreduction [9]. SDRs are involved in hormone metabolism (retinol dehydrogenases, prostaglandin dehydrogenases, hydroxysteroid dehydrogenases, testosterone 5α-reductases) fatty acid oxidation (hydroxyacyl CoA dehydrogenases) or biotransformation of xenobiotics (carbonyl reductases, quinone reductases) [10-13]. Interestingly, hydroxysteroid dehydrogenases (HSDs) of the SDR super-family are implicated in polycystic kidney diseases [14], regulation of blood pressure [15], Alzheimer's disease [16], obesity [17] and in the development of steroid dependent cancer forms [15]. The SDR superfamily therefore contains several important pharmaceutical targets. SDR family members including ADH from *Drosophila melanogaster* (*Dm*ADH) and *Scaptodrosophila lebanonensis* (*Sl*ADH) (formerly *Drosophila lebanonensis*) utilize nicotinamide adenine dinucleotides NAD(P)(H) as cofactors in the reduction or oxidation reactions. Currently there are around 300 x-ray crystal structures of SDRs in the protein data bank (www.pdb.org) [18], and 9 of them are of *Sl*ADH (Table 1).

Table 1. SlADHs structures available in the protein databank (www.pdb.org).

PDB ID	Ligand(s)	Resolution	Released Date	Number of amino acids	Reference
1A4U	-	1,92	16.02.1999	508	[19]
1B14	NAD+	2,4	26.11.1999	508	[20]
1B15	NAD-acetone	2,2	26.11.1999	508	[20]
1B16	NAD-3-Pentanone	1,4	29.11.1999	508	[20]
1B2L	NAD-Cyclohexanone	1,6	26.11.1999	254	[20]
1SBY	NAD+ and 2,2,2-trifluoroethanol	1,1	22.02.2005	508	[21]
1MG5	NADH and acetate	1,6	21.01.2005	510	[22]
3RJ5	NAD+	1,45	02.05.2012	508	[23]
3RJ9	NAD+	1,98	02.05.2012	1524	[23]

1.3 Reaction mechanism of DADH

Most of the SDR family members show a one-domain architecture with the substrate binding site located in the highly variable C-terminal region and a characteristic NAD(H)-binding motif or Rossmann fold in the N-terminal region. The overall structure of this monomer is folded into a central 8-stranded β-sheet and flanked on each side by three α-helices (Figure 1) [9, 19, 20, 22, 24, 25]. Among these enzymes, conserved sequence regions include the cofactor binding Gly-X3-Gly-X-Gly motif in the N-terminal part, and an active site conformation nearly superimposable to each other with the catalytic important triad (Tyr, Lys, Ser) of amino acids [9, 26, 27]. Mutagenesis studies have shown that these three residues are essential for catalytic activity [28-32].

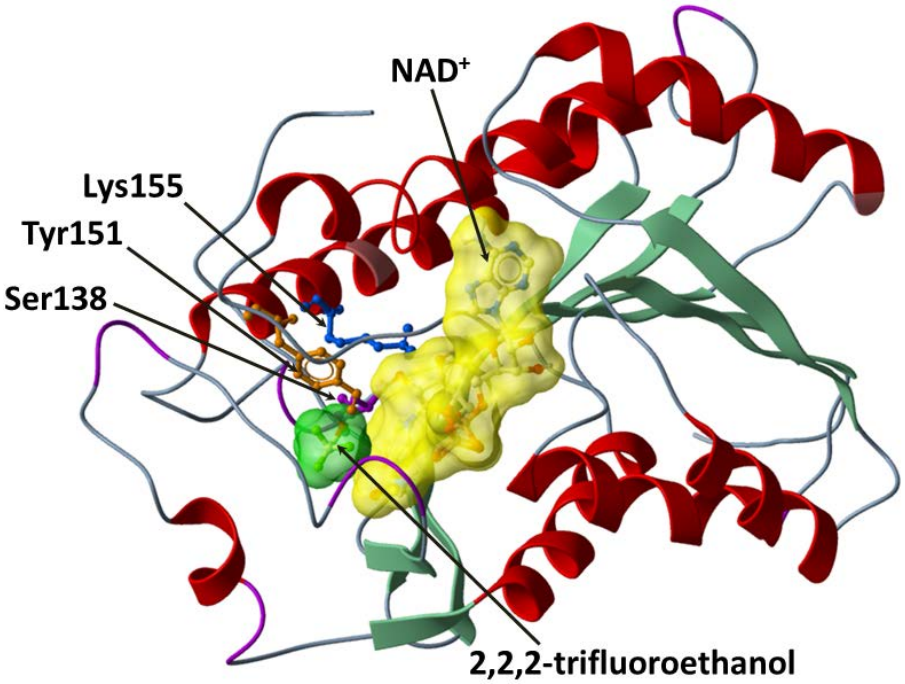

Figure 1: Skin mesh representation of substrate binding site (green) and the 'Rossmann-fold' (yellow) of *Sl*ADH in complex with NAD+ and 2,2,2-trifluoroethanol (PDB code: 1SBY).

Enzyme kinetic studies of *D*ADHs show that the SDR reaction appears to proceed through a two substrate compulsory mechanism (Scheme1) [27, 33], where the coenzyme binds before the substrate and the product disassociates before the coenzyme. As shown in scheme 1, a proton is released in the oxidation process of alcohols, while a proton is taken up in the reduction of aldehydes/ketones.

Alcohol + $NAD^+ \leftrightarrow$ aldehyde/ketone + NADH + H^+ (Scheme 1)

Enzyme kinetic studies of *D*ADHs have also shown that the proton is realised upon formation of the binary enzyme•NAD^+ (E•NAD^+) complex [27, 34, 35], and that most of the secondary alcohols tested are better substrates than the primary alcohols [36-38] . *D*ADH is a dimer of M_r 54800, consisting of two identical subunits [1, 39, 40].

The oxidation reaction of DADH includes two steps (Figure 2):

1. A proton transfer from the alcohol H_{Alc} atom to the strong base or nucleophile of the binary E•NAD^+ complex.
2. A hydride transfer from the alcohol H_{CAlc} atom to the C4 atom of NAD^+.

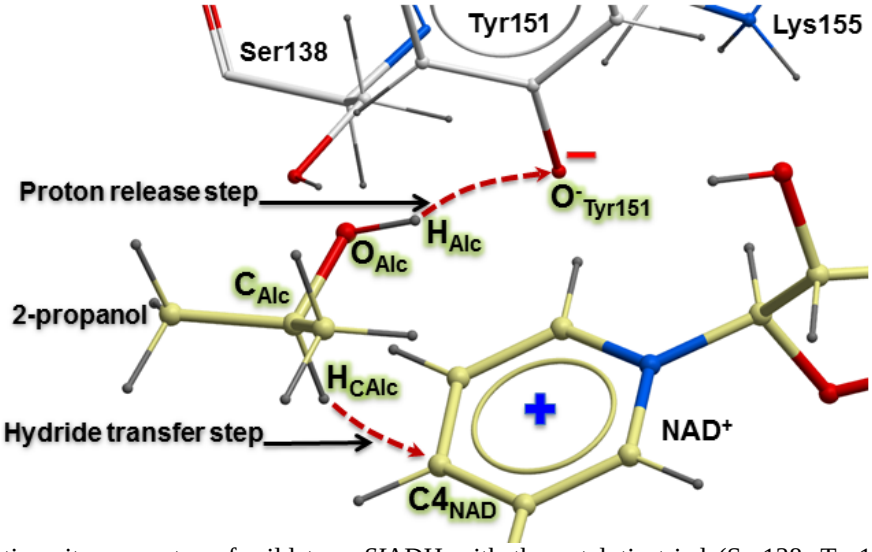

Figure 2: Active site geometry of wild type *SI*ADH with the catalytic triad (Ser138, Tyr151, Lys155), substrate 2-propanol and parts of NAD+ (PDB: 1SBY). Proposed oxidation reaction mechanism of 2-propanol by wild type *D*ADH.

The exact catalytic function of the catalytic triad is not known. Enzyme kinetic data have shown that in order to promote hydride transfer from the substrate alcohol to the NAD^+ molecule, the group (or combination of groups) showing a pK_a value of 7.1 in the E•NAD^+ complex has to abstract a proton from the C_α hydroxyl group of the substrate to generate an alcoholate anion R-CH_2-O^-. This group needs to be negatively charged in order to bind the substrate and facilitate hydride transfer from the substrate [27]. Due to its position in the active site and the pH dependence of alcohol binding, it was proposed that this group is the strictly conserved Tyr151 [19, 20, 31, 41-44]. It was suggested that the tyrosine function as the basic catalyst being fully negatively charged, and that the lysine binds NAD(P)(H) and lowers the pKa value of the tyrosine, while the serine stabilizes the substrate, reaction intermediates and product during catalysis [45]. The tyrosine is strictly conserved, whereas Ser and Lys are conserved in most SDRs [9].

However, this hypothesis has been challenged by an electrostatic analysis of the ionization properties of the active site residues in *D*ADH, using an approach which accounts for multiple locations of the hydrogen atoms of ionizable and polar groups [46]. Theoretical calculations showed that the protonation/deprotonation transition of the E•NAD^+ complex is related to the coupled, irregular ionization of the active site groups Tyr151 and Lys155.

1.4 Eight membered water chain in DADH

In protein crystal structures, it is now widely accepted that water molecules buried inside the protein play an important role in protein stability, dynamics and function [47, 48]. Water molecules trapped inside protein interiors can fill defects in the side chain packing or form hydrogen bonds to protein polar atoms [49, 50]. The number of water molecules included in the protein x-ray crystallographic models depends mainly on the resolution of the solved structure [51].

The exact range of processes mediated by buried water molecules in *D*ADH was not known, until 1998, then the x-ray crystal structure of *Sl*ADH (PDB Code: 1A4U) resolved at 1.9 Å resolution by Ladenstein and his colleagues showed three well-ordered water molecules in hydrogen bond distances to side-chains of the catalytic triad [19]. With an even higher resolution of the *Sl*ADH x-ray structure (PDB Code: 1B16), water molecules were also found between NAD^+ and the enzyme [20]. Based on these findings and kinetic studies, Koumanov and his colleagues proposed a proton relay chain which includes the active site catalytic residues, the O_2' ribose hydroxyl group of the coenzyme that plays a key role by acting as a proton switch, as well as a chain of eight water molecules that connects the active site with the bulk solvent [19, 20, 25, 33, 35, 37, 43, 46, 52-54] (Fig 3). Later research has shown that the water chain also exists in the ternary complex and that all amino acids lining the water are conserved in 119 *drosophilid* species. These findings support the hypothesis of a proton transport in between the active site and the solvent mediated by the relay chain [10], and it was suggested that this relay mechanism facilitate the proton abstraction from the binary E•NAD^+ complex [19, 20, 46]. A similar water chain has also been shown to exist in human and bacterial SDR enzymes [55-57]. This suggests that if not all, but at least part of these buried water molecules are conserved between proteins belonging to the same family and they are structurally and functionally important.

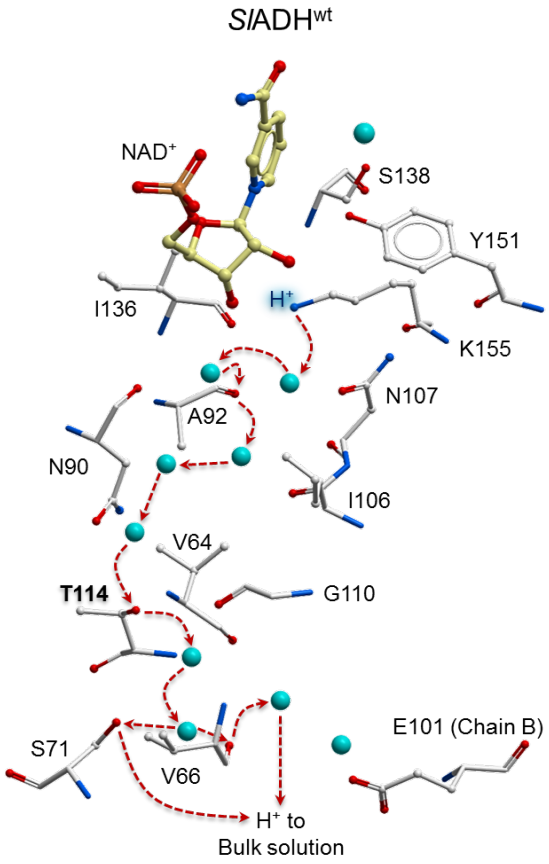

Figure 3: Structure of the water chain in *Sl*ADH wild type (PDB Code: 1SBY) at 1.1 Å resolution. The water molecules in the chain are shown as green balls and the amino acids involved in the putative proton relay system are shown in ball and stick. Dashed arrows show the putative proton transport from Lys155 through the water chain into the bulk solution.

1.5 SDRs as drug targets

Drosophilid has been studied for quite some time as a laboratory model for genetics in general and also applied into human diseases studies, like substance addiction, Alzheimer's disease and Parkinson's disease [58-60]. By 2002, the total number of predicted genes of *drosophila* melanogaster was 13601, among which the number of estimated druggable targets were 1714 [61]. Among more than 46,000 primary structures of SDR superfamily enzymes identified in sequence databases by 2010, more than 80 were found in human [8]. The similarities in sequences, function and protein structures within a gene family may often suggest that the binding-site architecture between family members is well conserved (Figure 4).

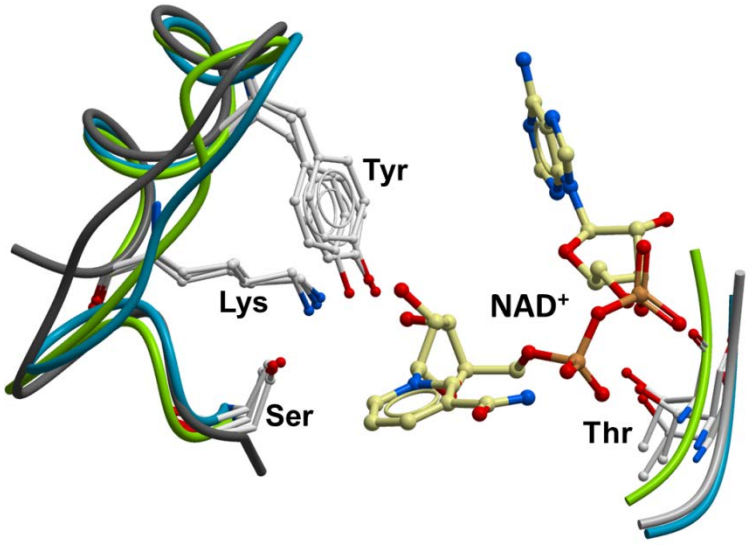

Figure 4: Protein worm representation of the active site of three SDRs from different family members. Grey colored protein worm is 17β-hydroxysteroid dehydrogenase type 1 (PDB code: 1FDT, residues displayed are Ser142, Tyr155, Lys159 and Thr189). Green colored protein worm is *Sl*ADH (PDB code: 1SBY, residues displayed are Ser138, Tyr151, Lys155 and Thr186). Blue colored protein worm is amyloid beta-peptide-binding alcohol dehydrogenase (PDB code: 1U7T, residues displayed are Ser155, Tyr168, Lys172 and Thr203).

This indicates that if one member of a gene family could bind a drug, other members with similar active site architecture and function may also be able to bind a compound with similar physio-chemical properties [8, 62, 63]. Therefore DADHs can be used as model system for the development of new therapeutic compounds targeting therapeutical important SDRs [14-17] . In the following I will give a brief introduction into the potential of some SDRs as drug targets.

1.5.1 17β-hydroxysteroid dehydrogenase type 1 and type 2 as drug targets in breast cancer

Breast cancer is a major cause of death in both European and American women, it occurs most frequently in post-menopausal women [64, 65] . 17-β-estradiol (E2) stimulates the growth of hormone-dependent breast cancer cells [66]. The precursor of E2 is oestrone (E1). The major enzyme catalyzing the reduction of E1 to E2 is 17-β-hydroxysteroid dehydrogenase type 1 (17-β-HSD1). The reverse reaction, the deactivation of E2 is catalyzed by 17-β-HSD type 2 (17-β-HSD2) (Figure 5) [67]. Both 17-β-HSD1 and 17-β-HSD2 belong to the family of SDRs requiring NAD(P)(H) as cofactor. They are present in healthy premenopausal women, but several studies have indicated that the ratio of 17-β-HSD1 to 17-β-HSD2 is increased in tumors of post-

menopausal women with hormone dependent breast cancer [68-70]. Studies have also indicated that that patients with high 17-β-HSD1 expression have significantly shortened disease-free and overall survival [71, 72], indicating that compounds that inhibit 17-β-HSD1 may be therapeutically beneficial in treatment of hormone dependent breast cancer in post-menopausal women [73, 74].

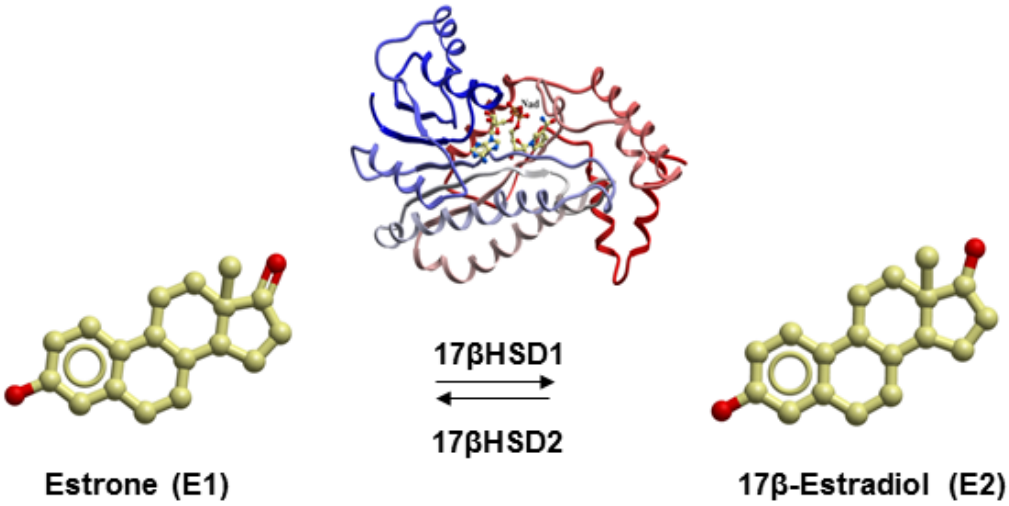

Figure 5: Inter-conversion of Estrone (E1) and 17 β-Estradiol (E2) catalyzed by 17-β-HSD1 or 17-β-HSD2.

Due to the structural and functional similarities of 17-β-hydroxysteroid dehydrogenase to other SDRs, the general information obtained from combination of theoretical calculations and experimental studies of SDRs from *D*ADHs as model systems can then be transferred to enzymes of the 17-β-HSDs family, and may be used for structural calculations of binding site geometry and inhibitors design of 17-β-HSD1 and (or) 17-β-HSD2.

1.5.2 Amyloid-β (Aβ) peptide-binding alcohol dehydrogenase as a target in Alzheimer's disease

Numerous studies have indicated the potential importance of amyloid-β peptide (Aβ) interaction with a mitochondrial enzyme called Aβ-binding alcohol dehydrogenase (ABAD), a member of SDRs family concentrated in mitochondria of neurons [75-82]. Aβ distorts ABAD's structure by forming Aβ-ABAD complex, thereby inactivate ABAD's metabolic functions and promotes Aβ-mediated cytotoxic events [83, 84]. Particularly, increased intracellular Aβ level prior to the appearance of neurofibrillary tangles and senile plaques in AD-affected areas of the brain suggested the role of Aβ in AD

development [83, 85-88]. An ABAD function inactivated *drosophilid scully* showed a developmentally lethal phenotype with multiple abnormalities [89]. Alternative term for ABAD is L-3-hydroxyacyl Coenzyme A dehydrogenase type II [90]. First human ABAD x-ray crystal structure was resolved by Kissinger and coworkers in 2004 (PDB code: 1U7T) [91]. Like other SDRs or ADHs, ABAD share the same active site features and utilize dinucleotide cofactor in catalytic reaction. In metabolic homeostasis, ABAD oxydize/reduce a wide range of substrate, such as linear alcohols, steroid substrates (17b-estradiol), S-acetoacetyl-CoA and β-hydroxybutyrate [90, 92]. ABAD appears to have cytoprotective functions under homeo-static conditions and in response to stress [93]. Studies of Yao et al. in 2011 showed inhibition of ABAD interaction with Aβ reduced Aβ accumulation and improved mitochondrial function in a mouse model of AD [94]. Therefore, ABAD could be a potential drug target. The x-ray crystal structure of ABAD is known suggesting that computer added drug design could be possible.

1.6 Enzyme kinetics

Until 2000, around 500 drug targets had been reported, among which 28% are enzymes [95]. However, only 120 drug targets are actually targeted by marketed drugs (47% are enzymes) [61]. Enzymes are powerful biological catalysts that are essential for the proper maintenance and reproduction of any organism. These properties make them excellent candidates as therapeutic targets to combat diseases. In this regard, one goal of molecular medicine is to develop and implement effective agents that can modulate the activities of various enzymes involved in essential biological pathways. Therefore, the process of drug development often requires accurate knowledge of the catalytic mechanism of the enzyme in question. In this study, we mainly focus on the mechanisms of two substrate enzymes.

1.6.1 Two substrate enzymes and their catalytic mechanisms

Enzymes like oxidoreductases, transferases and ligases catalyze reactions involving more than one substrate [96]. These enzymes utilize metal ion or organic cofactors as additional substrates. When it comes to the binding order of substrates for a two substrate reaction, there are mainly two types of mechanism: i) Ping-Pong/double

displacement mechanism/substituted enzyme mechanism, ii) ternary complex mechanism (Figure 6) [96-98].

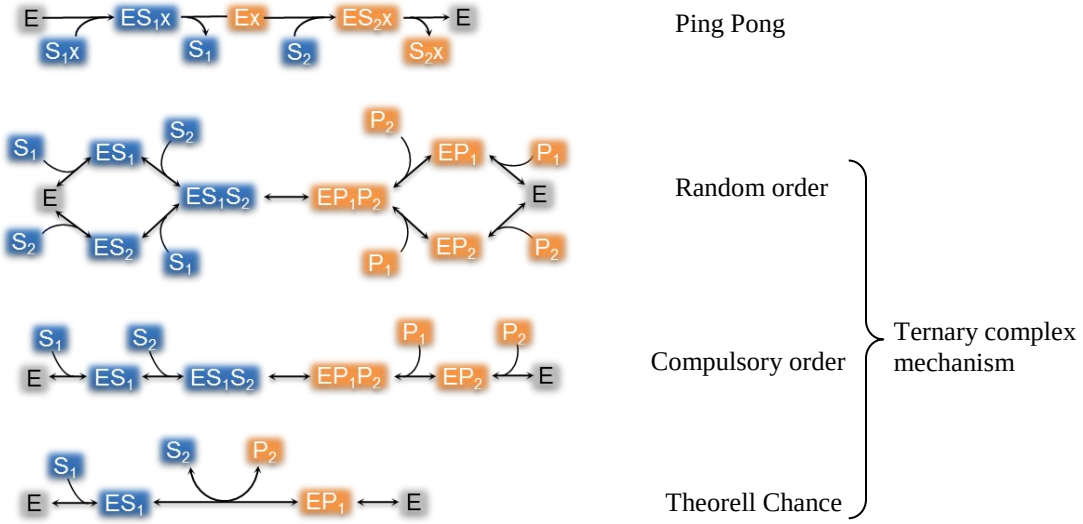

Figure 6: Example of catalytic mechanisms of two substrate enzymes. E: enzyme, S_1: substrate 1, S_2: substrate 2, P_1: product 1, P_2: product 2.

Ping-pong mechanism occurs when two substrate share one active site. In this case, one substrate leaves one moiety (phosphate group, an amino group or acyl group etc) on the enzyme to be transferred to the second substrate. In such a case, the two substrates do not bind to the enzyme at the same time during the reaction. In the other main type of mechanism, the ternary complex mechanism, both substrates must be bound to the enzyme at the same time and form a ternary complex (ES_1S_2) in order to start the catalytic reaction. There are various possibilities for the formation of a ternary complex. The binding of S_1 and S_2 either follows sequential order (compulsory-order mechanism), or they randomly binds to the enzyme (random-order mechanism). A special case of a compulsory-order mechanism occurs when the interconversion of ES_1S_2 and EP_1P_2 is much faster than all the other steps and no kinetically significant ternary complexes appear to occur. This is called a Theorell-Chance mechanism. Enzyme kinetic studies provide microscopic views of the factors affecting enzyme-catalyzed reactions. Chemical reactions involved enzymes can be quantitatively evaluated by measuring the speed at which the reacting substances are transformed to the corresponding products, namely reaction rate.

There are two types of kinetic studies that can be performed:

(1) Pre-steady state, which is the period when an enzyme-substrate complex is formed, there is sometimes some transiently formed enzyme-intermediate complex. This period lasts from micro- to milli-seconds. To be able to detect the formed enzyme•substrate (ES) complex and probable intermediates, one method is stopped-flow kinetics. The enzyme concentration used in this method is usually high and in the region of the used substrate concentration;

(2) Steady state, which is the period during the reaction where there is no change in the amount of the formed ES complex and other intermediates. This period often lasts from a fraction of a second to several minutes (sometimes hours). Furthermore, the enzyme concentration used is much lower than the used substrate concentrations [99, 100].

The reaction scheme including rate constant for compulsory-order mechanism was given as follows (Scheme 2):

$$E + S_1 \underset{k_2}{\overset{k_1}{\rightleftarrows}} ES_1 + S_2 \underset{k_4}{\overset{k_3}{\rightleftarrows}} ES_1S_2 \underset{k_6}{\overset{k_5}{\rightleftarrows}} EP_1P_2 \underset{k_8}{\overset{k_7}{\rightleftarrows}} EP_1 + P_2 \underset{k_{10}}{\overset{k_9}{\rightleftarrows}} E + P_1 \qquad \text{(Scheme 2)}$$

Where E is the enzyme, S_1 and S_2 are substrates, P_1 is the product from S_1 and P_2 is the product from S_2, ES_1 and EP_1 are binary complexes, ES_1S_2 and EP_1P_2 are ternary complexes, k_1 to k_{10} are rate constants. The catalytic mechanism and experimentally observed kinetic behavior can be mathematically expressed by a rate equation that depicts the process in terms of rate constant and reactant concentrations. The rate equation that describes the relation between kinetic coefficients and substrate concentrations can be written as equation (1) for a ternary complex mechanism and as equation (2) for a ping-pong mechanism using Dalziel nomenclature [101]:

$$\frac{e}{v} = \left[\varphi_0 + \frac{\varphi_1}{[S_1]}\right] + \frac{1}{[S_2]}\left[\varphi_2 + \frac{\varphi_{12}}{[S_1]}\right] \qquad \text{(Eqn.1)}$$

$$\frac{e}{v} = \varphi_0 + \frac{\varphi_1}{[S_1]} + \frac{\varphi_2}{[S_2]} \qquad \text{(Eqn.2)}$$

In these equations, *e* is the amount of active enzyme, v_0 is the initial rate of reaction, $[S_1]$ and $[S_2]$ are the concentration of substrate 1 and substrate 2, respectively. φ_0, φ_1, φ_2 and φ_{12} are kinetic coefficients. In two substrate reactions, the reaction rate *v* is dependent on the concentration of both S_1 and S_2. This algebraic rearrangement of the Michaelis-Menten equation is the mathematical basis for deducing Lineweaver-Burk type of plot [102]. Lineweaver-Burk analysis is one method of linearizing substrate-velocity data so that the kinetic coefficients can be determined by using primary and secondary plots (Fig 7) [101, 103].

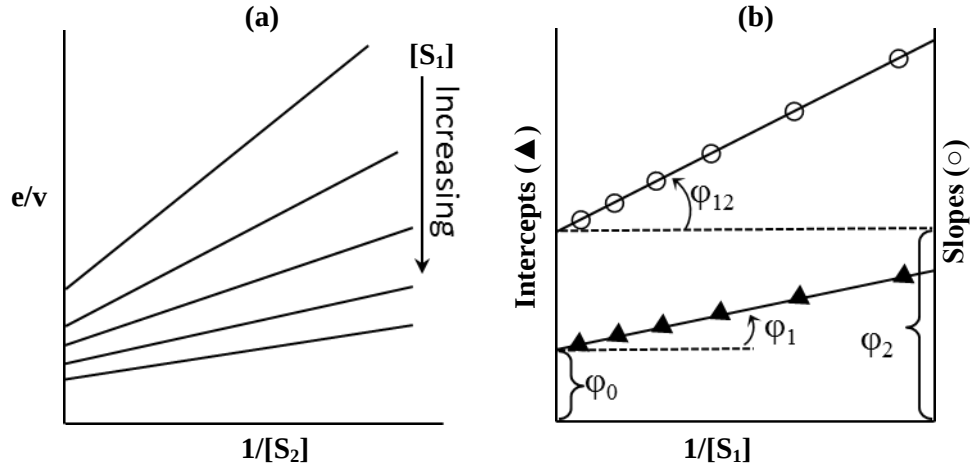

Figure 7: Plots illustrate the determination of the kinetic coefficients of equation (1) by secondary plots of slopes and intercepts (b) of primary Lineweaver-Burk plots (a).

In figure 2, a series of Y intercept and Slope values collected from plot (a) can then be introduced into equation (1), where from a secondary plot (b), the value of different φ coefficients can then be determined [96]. The physical meaning of φ coefficients in a compulsory ordered ternary complex mechanism is listed in Table 2.

Table 2: The meaning of different kinetic coefficients.

$1/\varphi 1$ (k_1 or k_{on})	**$1/\varphi 2$ (k_2 or k_{on})**	**$1/\varphi 0$ (k_{cat})**	**$\varphi 1/\varphi 0$**	**$\varphi 2/\varphi 0$**	**$\varphi 12/\varphi 1\ \varphi 2$, ($k_{off}$), k_{-1}**
Formation rate of ES_1 complex.	Formation and break down of the ternary complex	Production of the EP_1P_2 complex from ES_1S_2 and the release of products from the enzyme.	Km for S_1	Km for S_2	Disassociation rate of S_1 from the binary ES_1 complex

Not only can the characteristics of the rate equation and different kinetic coefficients verify the mechanism, conversely, the experimental observations provide clues to what the mechanism may be. Another way to verify the catalytic mechanism is to determine the reaction velocity in the presence and absence of inhibitors.

1.6.2 Enzyme Inhibition

Enzyme inhibitors may act either irreversibly or reversibly [100]. Irreversible inhibitors form covalent bonds with different functional groups on the enzyme surface. Reversible inhibitors form non-covalent interactions with various parts of the enzyme surface, which can be reversed by dilution and dialysis. Reversible inhibitors can either be products of the substrates investigated or other type of compounds. Reversible inhibitors can give rise to several types of inhibition patterns, and three such patterns are: competitive, uncompetitive and mixed inhibition. A product inhibitor pushes the reaction backwards while other compounds that react with a specific enzyme form and gives rise to an enzyme•inhibitor complex that is not a part of the flow from substrate to product is called a dead-end inhibitor [104]. It is common to use dead-end inhibitors in order to investigate the reaction mechanism of a multi substrate enzyme and if substrates bind and products leave in a specific order or not [100].

1.6.2.1 Dead-end inhibition

In 1962, Fromm and Zewe suggested that competitive inhibitors of substrates could be used to differentiate between random and ordered mechanisms [105]. Because dead-end inhibitors cannot reverse reaction sequences (as products for two substrate enzymes can), competitive dead-end inhibitors are often used to determine the enzyme's reaction mechanism, especially whether the substrates bind in a specific order or not [99, 104]. To get a full picture of the binding order of the two substrates to the enzyme, it is necessary to check the inhibitory pattern of each inhibitor against varied S_1 (fixed S_2) and varied S_2 (fixed S_1). In most cases one experiment is performed with low concentration of the fixed substrate (compared to its Km value) and another experiment with high concentration of the fixed substrate, while the other substrate is varied in the presence and absence of inhibitor. The inhibition patterns for a two substrate random and compulsory-order mechanism are shown in Figure 3 and 4. For a convenience, we

assume inhibitor I_1 only binds to the same site as substrate S_1, and inhibitor I_2 only binds to the same site as substrate S_2.

In a random order mechanism (Figure 8a), if I_1 or I_2 only binds to the free enzyme (E), then both S_1 and S_2 will compete with I_1 or I_2 for the free enzyme. Therefore, both inhibitors are competitive inhibitors against both substrates and will therefor give rise to four competitive patterns (not shown). If I_1 binds both to E and ES_2, then relative to S_1 (fixed S_2 concentration), I_1 shows a competitive pattern (Figure 8b), and relative to S_2, I_1 shows mixed inhibition (with low fixed S_1 concentration, Figure 8d). No inhibition occurs at a high fixed S_2 concentration. Similarly, If I_2 binds both to E and ES_1 (Figure 8a), then relative to S_2 (fixed S_1 concentration), I_2 shows a competitive pattern (Figure 8e), and relative to S_1, I_2 shows mixed inhibition (with low fixed S_2 concentration, Figure 8c). No inhibition occurs at a high fixed S_1 concentration. In short, if both inhibitors bind to free enzyme and their corresponding binary complex, it will give two competitive patterns (i.e. I_1 vs S1 and I_2 vs S_2 in Figure 8b, e) and two mixed patterns (i.e. I_1 vs S_2 and I_2 vs S_1 in Figure 8c, d). An uncompetitive pattern will never occur with a random order mechanism.

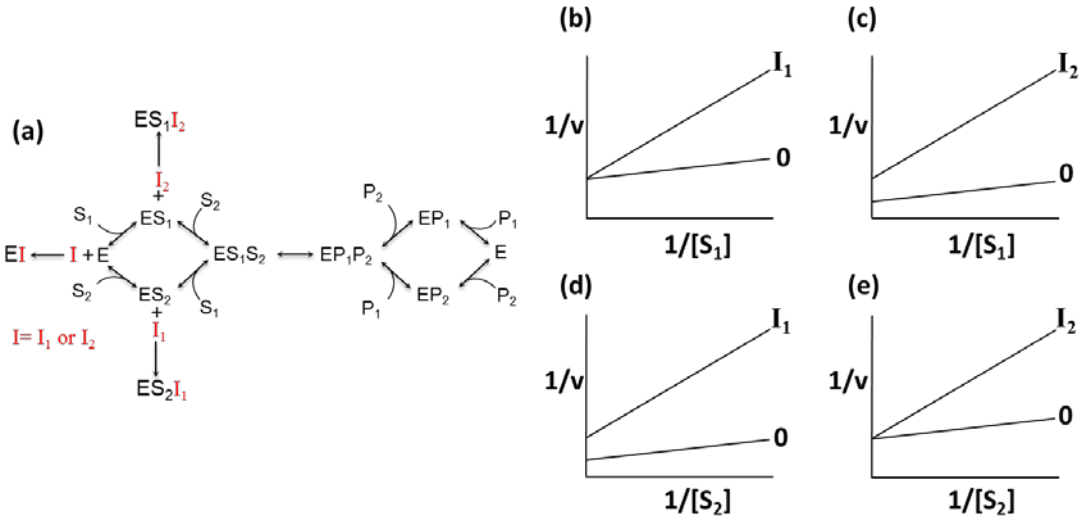

Figure 8: (a) Reaction scheme for a random-ordered mechanism where S_1 binds to the free enzyme E and ES_2, and S_2 also binds to the free enzyme and the binary ES_1 complex. Inhibitor 1 (I_1) binds to E and binary ES_2 complex, I_2 binds to E and binary ES_1 complex. (b-e) double invers plots of v vs a varied substrate in the absence (0) and presence (I_1 or I_2) of inhibitor. Inhibition pattern of I_1 vs varied $[S_1]$ (b) and I_2 vs vaired $[S_1]$ (c) using a fixed $[S_2]$. Inhibition pattern of I_1 vs varied $[S_2]$ (d) and I_2 vs vaired $[S_2]$ (c) using a fixed $[S_1]$.

In a compulsory ordered mechanism (Figure 9), when a competitive dead-end inhibitor I_1 binds to the free enzyme, it distorts the enzyme so that substrate S_1 cannot bind to the EI_1 binary complex. This makes the inhibitor I_1 to compete with the substrate S_1 (Figure 9b) and it will give a mixed inhibition against substrate S_2 (Figure 9d). On the other hand, inhibitor I_2 competes with substrate S_2 (Figure 9c) and does not bind to the free enzyme, only to the ES_1 binary complex (Figure 9a). In this mechanism, inhibitor I_2 shows an uncompetitive pattern against substrate S_1 (Figure 9c). This unique uncompetitive pattern of I_2 helps to distinguish a compulsory ordered mechanism from a random ordered mechanism. Similarly, I_1 shows mixed inhibition pattern against varied S_2 which means that the inhibitor binds before the varied substrate S_2 and that there is a reversible connection between EI_1 and ES_1 as shown in Fig 9a [104].

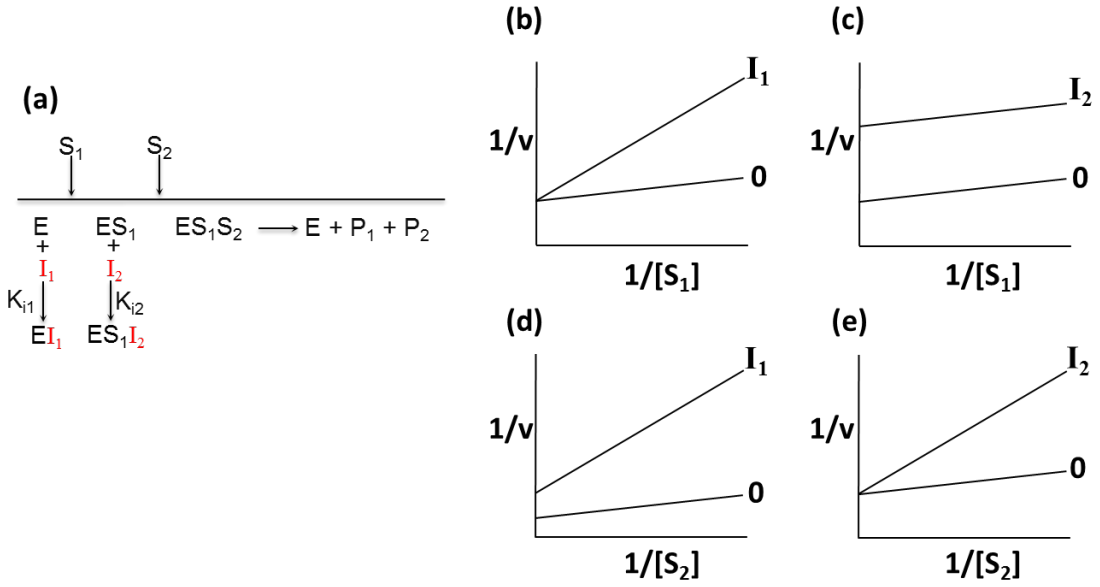

Figure 9: Reaction scheme for a compulsory ordered mechanism where S_1 binds to the free enzyme E and S_2 to the binary ES_1 complex. Inhibitor 1 (I_1) binds to E and I_2 to the binary ES_1 complex. (b-e) double invers plots of v vs a varied substrate in the absence (0) and presence (I_1 or I_2) of inhibitor. Inhibition pattern of I_1 vs varied $[S_1]$ (b) and I_2 vs vaired $[S_1]$ (c) using a fixed $[S_2]$. Inhibition pattern of I_1 vs varied $[S_2]$ (d) and I_2 vs vaired $[S_2]$ (c) using a fixed $[S_1]$.

1.6.3 Enzyme-inhibitor dissociation constants

The equilibrium dissociation constant of an enzyme•inhibitor (EI) complex can be derived from inhibition kinetic studies, and is then called an inhibition constant, K_i [103]. An obtained K_i value from kinetic studies will either be a true dissociation

constant ($K_i = K_d$) or an apparent constant ($_{app}K_i$: i.e. $K_i \neq K_d$) [103]. This depends on the kinetic mechanism and the experimental conditions used.

For a compulsory ordered two substrate reaction where S_1 binds to the free enzyme and a dead-end inhibitor also binds to free enzyme (Figure 9a), then equation (1) becomes:

$$\frac{e}{v} = \varphi_0 + \frac{\varphi_2}{[S2]} + \frac{1}{[S1]}\left(\varphi_1 + \frac{\varphi_{12}}{[S2]}\right)\left(1 + \frac{[I_1]}{K_{i1}}\right) \quad \text{(Eqn.3)}$$

If the concentration of S_2 is fixed, then the obtained K_{i1} value from the slope of equation (3) represents the true dissociation constant (K_d) of the EI complex. This is independent of the concentration of the fixed substrate (in this case S_2).

If competitive dead-end inhibitor binds only to the ES_1 binary complex (Figure 9a), then equation (3) becomes:

$$\frac{e}{v} = \varphi_0 + \frac{\varphi_1}{[S_1]} + \frac{1}{[S_2]}\left[\varphi_2\left(1 + \frac{[I_2]}{K_{i2}}\right) + \frac{\varphi_{12}}{[S_1]}\right] \quad \text{(Eqn.4)}$$

Inhibitor I_2 competes with substrate (S_2). In this case, the obtained inhibitor constant K_{i2} does not necessarily represent the true dissociation constant of the ES_1I_2 complex. The reason for that is simply that I_2 binds to the ES_1 complex. At a low concentration of S_1, only small amounts of the enzyme are in the form of the binary ES_1 complex to which I_2 can bind. Then the obtained binding constant is weaker than the true binding constant, i.e. K_{i2} is larger than K_d. At an infinite (or high enough) concentration of the fixed substrate S_1, $\frac{\varphi_{12}}{[S1]} \approx 0$, the obtained K_{i2} value can represent the true dissociation constant of the ternary ES_1I_2 complex. This is because the entire amounts of enzyme are in the binary ES_1 complex. With a saturating concentration of S_1, the strength of the EI complex (K_i) calculated from the slop term (K_{is}) can be determined from equation (5) [33]:

$$K_{is} = \frac{[I]}{\frac{s_i}{s_0} - 1} \quad \text{(Eqn.5)}$$

Where [*I*] is the inhibitor concentration, s_i and s_0 are inhibited and uninhibited slopes in a Lineweaver-bruke plot (Figure 9e), respectively. Here, K_{is} can be regarded as the dissociation constant of I_2 from the ternary complex (ES_1I_2). K_i can also be calculated from plot in Figure 9c using intercept term (K_{ii}). The corresponding equation using the intercept term will be:

$$K_{ii} = \frac{[I]}{\frac{i_i}{i_0} - 1} \qquad \text{(Eqn.6)}$$

Where i_i and i_0 are the inhibited and uninhibited intercepts. As I_2 binds to the ES_1 binary complex, the mathematical correlation between K_d, K_i and the kinetic coefficients using the Dalziel nomenclature is shown in equation (7) by using equation (5):

$$K_d = \frac{K_{is}}{\left(\frac{\varphi_{12}}{\varphi_2[S_1]} + 1\right)} \qquad \text{(Eqn.7)}$$

Or by using equation (6):

$$K_d = \frac{K_{ii}}{\left(\frac{\varphi_0[S_2]}{\varphi_2} + 1\right)} \qquad \text{(Eqn.8)}$$

From equation (8) it obvious that if a high enough concentration of S_1 is used ($\frac{\varphi_{12}}{\varphi_2[S_1]} \approx 0$), then the obtained $K_i = K_d$. In all other situations the obtained K_i is an apparent dissociation constant ($_{app}K_i$) which is larger than K_d. The larger the K_d the weaker the binding. If the kinetic coefficients (k_{cat}, K_m or different φ value) for the reaction are known, and a K_i value has been obtained from equation (5) using a fixed $[S_1]$, the true dissociation constant K_d can be calculated from equation (7).

1.7 Application of Molecular modeling in enzyme kinetic studies

1.7.1 Docking and scoring

Modern drug discovery often include searching for small molecules that can bind to a preselected protein target. Protein-ligand docking aims to predict and rank binding orientation of ligands in a target protein of known 3D structure [106]. Starting from the early 1980's [107], it remains a field of vigorous research, having become a useful tool in drug discovery programs [108]. The protein-ligand docking occupies a very special place in the field of docking, because of its applications in medicine [109]. From the docking of both protein and ligand as rigid bodies [107], protein-ligand docking has developed to an area where full flexibility on the ligand is commonly included. Although binding orientation and affinity of a given ligand, and binding-site geometry of target protein can be greatly influenced by protein flexibility [110], including protein flexibility is still a challenge and computationally expensive by most docking programs. The traditional lock-and-key and induced-fit theories have given their way to more modern theories that bestow a greater weight to the receptor flexibility issue [111]. The current idea interprets a protein as an ensemble of differently populated conformational states in equilibrium, rather than the stable conformation appearing in X-ray crystal structure [111]. An important notion that needs attention is that the conformations of the target protein in the protein-ligand complex are not necessarily the most populated conformations in an unbound state [110-112]. So, when it comes to docking, these aspects imply that instead of targeting a single pose of a given ligand on a single target protein structure, one should ideally look for the most populated alternatives from an ensemble of solutions comprising several different binding conformations [106]The docking result are mainly judged by two factors: (1) the ability to make key hydrogen bonding and hydrophobic contacts and (2) the ability to achieve a reasonable root-mean-square deviation (RMSD) which is lower than 2 Å after redocing compounds found in X-ray crystal structure complexes [113].

Molecular-docking ultimately seeks to predict the best mode by with a given compound will fit into a binding site of a macromolecular target. As a result, this usually involves two independent steps:

- Docking: Determining the orientation of a ligand relative to the receptor.

- Scoring: Evaluate the ligand orientation.

Scoring is used to evaluate the interaction between a ligand and its target protein by ranking how well the ligand fit into the binding pocket or by predicting the absolute binding affinity between the ligand and its target protein. Although the standard free energy of binding (ΔG) is given by the Gibbs Helmholtz equation (equation 9) [100], the predicted binding affinity in terms of ΔG is still an approximation.

$$\Delta G = \Delta H - T\Delta S = -RT \ln K_i \qquad \text{(Eqn.9)}$$

Where ΔH is the enthalpy, T is the temperature (Kelvin), ΔS is the entropy, K_i is the binding constant and R is the gas constant [114].

1.7.2 Glide docking program

Glide (Grid-based Ligand Docking with Energetics) is one of the most widely used docking programs. The Glide algorithm approximates a systematic search of positions, orientations, and conformations of the ligand in the protein-binding pocket via a series of hierarchical filters. The procedure of how Glide works is illustrated in Figure 10.

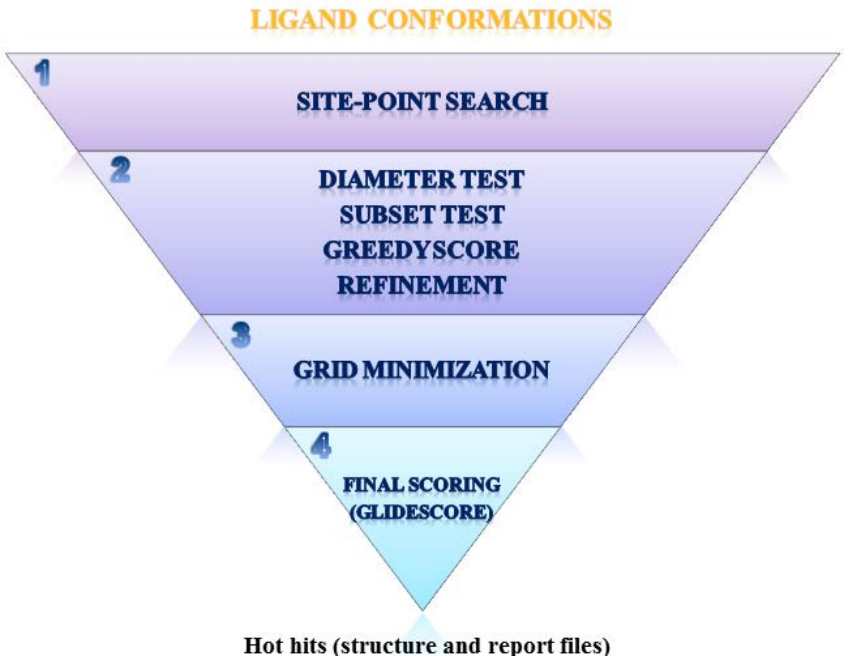

Figure 10: Glide docking procedure in four stages.

A typical scoring function contain terms like:

$$\Delta G_{score}=\alpha_1\Delta E_{vdw}+ \alpha_2\Delta E_{H\text{-}bond+} \alpha_3\Delta E_{el+} \alpha_4\Delta E_{rot+} \alpha_5\Delta E_{solv} +\ldots \quad \text{(Eqn.10)}$$

Here α_i is weighting factors that can be fitted to actual binding data of specific protein-ligand systems. The scoring in Glide 5.7 is first carried out in 'Greedy score' stage using Schrödinger's ChemScore empirical scoring function [115]. Much as for ChemScore [116], this algorithm recognizes favorable hydrophobic, hydrogen-bonding, and metal-ligation interactions, and penalizes steric clashes. Only a small number of best refined poses are transferred to next stage that involves evaluation and minimization of a grid approximation to the OPLS-AA non-bonded ligand-receptor interaction energy [117, 118]. Finally, the minimized poses are re-scored using Schrödinger's proprietary GlideScore scoring function:

$$G_{Score} = 0.065*vdW + 0.130*Coul + Lipo + Hbond + Metal + BuryP + RotB + Site \quad \text{(Eqn.11)}$$

Here *vdw* stands for van der Waals energy, *Coul* is the Coulomb energy, *Lipo* is the lipophillic contact term, *Metal* is the metal binding term where only the interactions with anionic acceptor atoms are included, *BuryP* is the penalty for buried polar groups, *RotB* is the penalty for freezing rotatable bonds, and *Site* is the polar interactions in the active site. GlideScore is based on ChemScore, but includes a steric-clash term and adds buried polar terms devised by Schrödinger to penalize electrostatic mismatches.

Before initiating the ligand docking, a receptor grid maps must be generated. The grid files represent physical properties of a volume of the target protein (specifically the active site) that are searched when attempting to dock a ligand. First, the prepared structures (both protein and ligand) are imported. The receptor is selected by excluding the ligand, while the active site can be defined as the centroid of the ligand. To increase the docking accuracy, different constrain can be added. For example, a hydrogen bond constrain can be set between the ligand and an active site amino acid or cofactor of the target protein. Other constrains like bond angle and atom position can also be used. The calculated target protein grid file is then used to dock the ligands with standard precision (SP), high throughput virtual screening (HTVS) or extra precision (XP) docking modes. In Glide XP docking, another scoring function called XP Glide-ChemScore [119] is used. This scoring function includes additional terms over the SP scoring function, and a more complete treatment of some of the SP terms.

1.7.3 Molecular Mechanics

The molecular modeler often wants to understand and predict properties of liquids, solutions, solids and macromolecules. The experimental properties of a system such as the pressure and the heat capacity are determined by the positions and momentas of the particles that comprise the system. So the word simulation in turn refers to methods aimed at generating a representative sampling of a system at a finite temperature, volume and pressure.

Molecular mechanical methods can be used to search energy minimum of a molecular system and simulate molecular behavior. The two main simulating methods using molecular mechanics are Monte Carlo (MC) and Molecular Dynamics (MD). These simulation methods can be used to overcome energy barriers and find global energy minimum and to study random or time dependent structural changes in a molecular system. Molecular mechanics calculations are using force fields (also named force field methods), and ignore the electronic motions and calculate the energy of a system as a function of the nuclear positions only. Basic functional form of a force field encapsulates both bonded terms relating to atoms that are linked by covalent bonds, and non-bonded (also called "non-covalent") terms describing the long-range electrostatic and van der Waals forces (Figure 11).

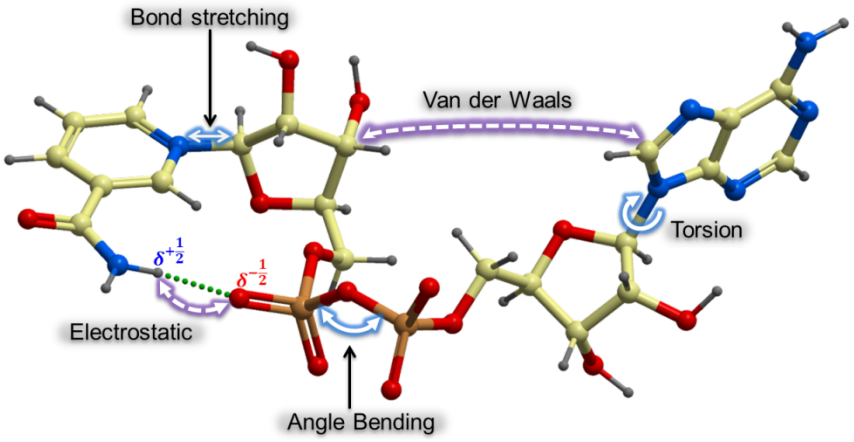

Figure 11: Representation of the key contributions to a molecular mechanics force field: bond stretching, angle bending and torsional terms, as well as non-bonded terms (Electrostatic and Van der Waals interactions). The molecular in this figure is NAD^+.

The force field can be written as [114]:

$$E_{total} = E_{bonded} + E_{nonbonded}$$

$$E_{bonded} = E_{bond} + E_{angle} + E_{dihedral}$$

$$E_{nonbonded} = E_{electrostatic} + E_{vanderwaals}$$

The total potential energy (E_{total}) is the sum of covalent (E_{bonded}) and non-covalent ($E_{nonbonded}$) bonding energy terms. E_{bonded} represent the sum of bond stretching (E_{bond}), angle bending (E_{angle}) and torsional energy ($E_{dihedral}$) terms. $E_{nonbonded}$ refers to electrostatic ($E_{electrostatic}$) and Van der Waals ($E_{vanderwaals}$) energy terms. A force field defines a set of parameters for each type of atom. For example, OPLS-AA has a functional form [120]:

$$E = \sum_{bonds} K_r(r - r_{eq})^2 + \sum_{angles} K_\theta(\theta - \theta_{eq})^2 + \sum_i \frac{V_1^i}{2}[1 + \cos(\varphi_i + f_i 1))] + \frac{V_2^i}{2}[1 - \cos(2\varphi_i + f_i 2))] + \frac{V_3^i}{2}[1 + \cos(3\varphi_i + f_i 3))] + \sum_i^{on\ a} \sum_j^{on\ b} \left[\frac{q_i q_j e^2}{r_{ij}} + 4\epsilon_{ij}\left(\frac{\sigma_{ij}^{12}}{r_{ij}^{12}} - \frac{\sigma_{ij}^{6}}{r_{ij}^{6}}\right)\right] f_{ij} \quad \text{(Eqn. 12)}$$

In this equation, the first three terms comprise bonded interactions, while the last term describes the nonbonded ones. The first and second terms represent the bond and angle terms, in which K_r and K_θ are the bond force constants and valence angle force constant. r_{eq} and θ_{eq} are equilibrium values for bond distance and valence angle, respectively. The third part represent the torsional energy terms between atom pairs i and j (i<j), in which φ_i is the dihedral angle, V_1, V_2, and V_3 are the coefficients in the Fourier series, and f_1, f_2, and f_3 are phase angles. The total torsional energy is then the sum of this series for each dihedral angle. The sums for the bonded terms are carried out over all atoms involved. The intermolecular nonbonded interaction energy between atoms i and j are represented by the Coulomb plus Lennard-Jones terms in the last part of the equation, in which q_i and q_j are the partial charges of the atoms i and j involved and e is the vacuum dielectric constant. ε_{ij}, σ_{ij}, f_{ij} and r_{ij} represent the well depth, collision diameter, scaling factor and the distance between the atoms i and j. The scaling factor f_{ij} equals 0.5 for 1,4 interactions and one otherwise. The non-bonded term is calculated between all pairs of atoms (i and j) that separated by at least three bonds.

1.7.3.1 Global energy minimum

In molecular modeling we are especially interested in minimum points on the energy surface. Minimum energy arrangements of the atoms correspond to stable states of the system, any movement away from a minimum gives a configuration with a higher energy [114]. The minimum with the very lowest energy is known as the Global energy minimum. The way in which the energy varies with the coordinates is usually referred to as the potential energy surface. Most optimization methods try to determine the minima point, but for a large system, the potential energy is a complicated, multi-dimensional function of the coordinates. Therefore, energy landscapes for large system are extremely complex, and finding a minima can be a challenging task, finding the global minimum is even more challenging [121, 122]. Many variables are used in computational chemistry optimization methods. Basically all methods assume that the first derivative (i.e. the gradients) of the function with respect to all variables can be calculated. More sophisticated methods also assume the second derivative matrix, the Hessian matrix (force constant matrix) [123], can be calculated. Most commonly used global minimum searching algorithm includes: steepest descent (SD) method, conjugate gradient (CG) method and Newton-Raphson (NR) method [114]. CG and SD minimizations operate in Cartesian space rather than internal coordinates. They are much faster than the other methods. As a second derivative method, NR method uses not only the first derivative but also the second derivative (i.e. the Hessian matrix) to locate a minimum. Due to large amount of calculation of the full second derivative matrix which must be stored and inverted, this can be computationally demanding for systems with many atoms. Hence, the NR method is more suited to small molecules (usually less than 100 atoms or so).

1.7.3.2 Monte Carlo simulations

Monte Carlo (MC) statistical mechanics methods typically employ a classical potential energy function for bond stretching, angle bending, torsions, and non-bonded interactions [124]. A MC simulation generates a new configuration by a set of random motions. The difference in energy between the new and the old configuration is used as a selection criterion by the Metropolis algorithm [125], which enforces a correct Boltzmann distribution of energies for the system at the desired temperature, and the procedure is then iteratively repeated until the minimum energy conformation is found.

Although MC methods have the advantage of using energy as basic information and random sampling of coordinates, sampling for large flexible molecules can be problematic since degrees of freedom will increase. The MC method doesn't consider atomic velocities and the time dimension.

1.7.3.3 Molecular dynamics simulations

The MD method calculates the time dependent behaviour of a molecular system. It is based on Newton's second law or the equation of motion, $\boldsymbol{F_i=m_ia_i}$, where $\boldsymbol{F_i}$ is the sum of all forces exerted on atom $\boldsymbol{i}$ that results in its acceleration $\boldsymbol{a_i}$, $\boldsymbol{m_i}$ is its mass. From knowledge of the force on each atom, it is possible to determine the acceleration of each atom in the system. The acceleration is the second derivative of the position with respect to time:

$$a_i = \frac{dv_i}{d_t} = \frac{d^2 r_i}{dt^2} \qquad \text{(Eqn.13)}$$

In words, it is the rate of change of the velocity $\boldsymbol{v_i}$, which in turn, is the rate of change of the position $\boldsymbol{r_i}$. Integration of the equations of motion then yields a trajectory that describes the positions, velocities and accelerations of the particles as they vary with time. From this trajectory, the average values of properties can be determined.

The MD method was first introduced by Alder and Wainwright in the late 1950's [126, 127] to study the interactions of hard spheres. Many suggestions concerning the behaviour of simple liquids emerged from their studies. The next major advance was in 1964, when Rahman carried out the first simulation using a realistic potential for liquid argon [128]. The behaviour of the particles in hard-sphere potential moves straight in lines at constant velocity between collisions. The collisions are perfectly elastic and occur when the separation between a pair of spheres equals the sum of their radii [114]. This simple model of hard spheres has given useful insights into hard-sphere particle movements, but is obviously not ideal for simulating atomic or molecular systems.

The first MD simulation of a realistic system was done by Rahman and Stillinger in their simulation of liquid water in 1974 [129]. The first protein simulations appeared in 1977 with the simulation of the bovine pancreatic trypsin inhibitor (BPTI) [130]. Today in the literature, one routinely finds MD simulations of solvated proteins, protein•DNA complexes as well as lipid systems addressing a variety of issues including the

thermodynamics of ligand binding and the folding of small proteins. MD techniques are also widely used as a supplement to experimental procedures such as X-ray crystallography and NMR structure determination. MD simulation can fold extended sequences to global potential energy minima for very small systems (peptides of length ten, or so, in vacuum) [131, 132], but it is most commonly used to simulate the dynamics of known structures.

The number of simulation techniques has greatly expanded; today there exist many specialized techniques for particular problems, including mixed quantum mechanical - classical simulations (i.e. quantum mechanics and molecular mechanics) that are being employed to study enzymatic reactions in the context of the full protein [133].

1.7.4 Combined quantum mechanics and molecular mechanics

One of the main problems in computational chemistry is to find a balance between the accuracy of the results and the computational cost. However, it is often not possible to increase the accuracy of the calculation when large systems are considered. The idea of combining different computational methods starts with the realization that various regions of the system play very different roles in macro-biomolecules. Examples of such are most enzymatic reactions, where the bond breaking and forming takes place only at the active site. Therefore, the expensive computational methods can be used for the part of the system where the action takes place, while less expensive methods can be used for the supporting regions. In 1976 Warshel and Levitt introduced a hybrid quantum mechanics and molecular mechanics (QM/MM) methods that treated the active part of the system using a quantum mechanical representation while the rest of the system was represented by an empirical force field [134].

Quantum physics provides a mathematical description of the wave/particle duality and interactions of energy and matter. It departs from classical physics, primarily at the atomic and sub-atomic scales. Quantum mechanics (QM) explicitly represents the electrons in a calculation, and so it is possible to derive properties that depend upon the electronic distribution and, in particular, to investigate chemical reactions in which bonds are broken and formed [114]. However, QM methods are limited to systems of up to a

few hundred atoms. The application and evaluation of QM/MM method against experimental data started only after 1990s [135-139].

1.7.4.1 General principles

The basic idea by using the hybrid methods is that a system is partitioned into several regions. The simplest approximation is to divide the system into three regions: a QM region, an MM region and the boundary region between QM-MM region (Figure 12).

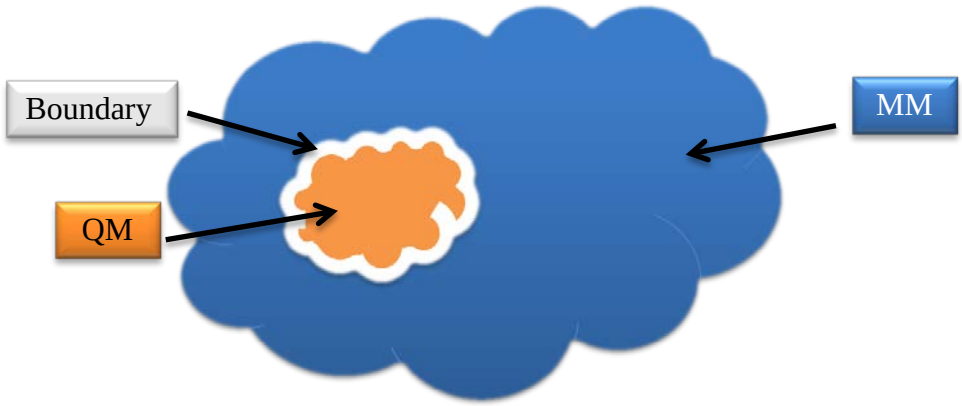

Figure 12: Defining the bio-molecular system into QM, MM and boundary regions.

Because of the strong interaction between QM and MM region, the total energy of the entire system cannot be written simply as the sum of the energies of these regions. Special precautions have to be taken at the boundary region, especially if it cuts through covalent bonds. Depending on the type of QM/MM method, this boundary may contain additional atoms (link atoms) that cap the QM region, or it may consist of atoms with special features that appear in both the QM and the MM calculations. Table (3) shows the most commonly used methods for these three regions and reference of their applications.

Table 3: The commonly used methods applied on the QM regions, MM regions and boundary regions

QM region	Density function theory (DFT) [140] , Hartree-Fock (HF) [141, 142], Møller-Plesset perturbation theory (MP) [143-145], Austin model 1 (AM1) [146-150], parametric method number 3 (PM3) [151-153], Self-consistent charge density-functional tight binding method (SCC-DFTB) [154-157], INDO/S-CIS method [158, 159], symmetry-adapted cluster−configuration interaction method (SAC−CI) [160-162], time-dependent DFT (TD-DFT) [163-165], multi-configuration *ab initio* methods (e.g., CASSCF or CASPT2) [166-168], Multi-reference *ab initio* methods (e.g., MRCI) [169]
Boundary region	Link atom method [135, 170], boundary-atom method [171-175], frozen localized orbital method [134].
MM region	AMBER [176-178], CHARMM [179-181], OPLS-AA [120, 182], GROMOS [183], EFP [166], UFF [143, 184-186]

1.7.4.2 The QM/MM energy expression

Two types of QM/MM energy expression schemes are described in the literature [187]: the additive and subtractive schemes.

The basic energy equation for an additive QM/MM scheme has been mentioned by Warshel and Levitt [134], Field, Bash and Karplus [135], Singh and Kollman [170]:

$$E_{QM/MM}^{add} = E_{MM} + E_{QM} + E_{QM-MM} \quad \text{(Eqn.14)}$$

Where E_{MM} is the energy of MM region, E_{QM} is the energy of QM region, E_{QM-MM} is the QM-MM coupling term or interaction energy between QM and MM region in the boundary region. When E_{MM} is considered in the force field, E_{QM-MM} term includes bonded, van der Waals, and electrostatic interactions between QM and MM region:

$$E_{QM-MM} = E_{QM-MM}^{bond} + E_{QM-MM}^{vdw} + E_{QM-MM}^{el} \quad \text{(Eqn.15)}$$

Most of the QM/MM methods presently in use (including the method in this study) are of the additive type.

A subtractive QM/MM energy equation was described by Morokuma and co-workers [188] :

$$E_{QM/MM}^{sub} = E_{MM}^{sys} + E_{QM} - E_{MM}^{QM} \quad \text{(Eqn.16)}$$

Where E_{MM}^{sys} is the energy from MM calculation of the entire system, E_{QM} is the energy of QM region, E_{MM}^{QM} is the energy of MM calculation on the QM region. The advantage of subtractive scheme is its simplicity, which means no explicit QM-MM coupling terms (Equation 14) are needed. On the other hand, the disadvantage is that handling the boundary region totally at MM level is particularly problematic when electrostatic interaction exists.

1.7.4.3 Application of QM/MM method

A large amount of work has to be done to perform QM/MM calculation; this includes the preparation of the system before the actual QM/MM calculations are taking place and the appropriate combination of QM and MM methods, as well as the treatment of the boundary region. Although errors and wrong choices from the beginning can hardly be recovered at the later stages, the unique features and promising accuracy of these methods have attracted many researchers for its application in studies of chemical reactions. Some excellent agreements were obtained between experimental studies and theoretical QM/MM calculations. These examples include reaction barriers studies of chorismate mutase (CM) and para-hydroxybenzoate hydroxylase (PHBH) [189], and the catalytic reaction mechanism of cytochrome P450cam [190]. Since QM/MM methods were introduced into enzymatic reaction studies about 30 years ago, the number of publications has been rapidly growing covering a wide range of bio-molecular systems, such as oxidoreductases [191-199], transferases [142, 144, 200-202], hydrolases [203-205], lyases [206-208], isomerases [146, 147, 209-214], photoactive proteins [163, 215-220], oligonucleotides and adducts [187, 221-229].

2 Aims of study

Several therapeutically important drug targets of the SDR family have large structural similarities with *Dm*ADH and *Sl*ADH. That indicates that *Dm*ADH and *Sl*ADH can be used as model systems for therapeutically important SDRs. Insight into the structure and function of *Dm*ADH and *Sl*ADH may therefore contribute with valuable knowledge for the development of new drugs targeting SDRs. We and others have been studying the enzymatic mechanisms and structure of *Dm*ADH and *Sl*ADH for years [19, 21, 22, 25, 33, 35, 37, 43, 52-54, 230], and a quit clear picture about how these enzymes function has been obtained. However, there are still puzzles that need to be solved.

All *D*ADHs contain an eight-membered water chain connecting the active site with the solvent at the protein surface. A similar water chain has also been shown to exist in other SDR enzymes including therapeutically important SDRs. The role of this water chain in the enzymatic reaction is unknown, but it has been proposed to be involved in a proton relay system facilitating proton transport between the active site and the solvent [46]. Previously, site-directed mutagenesis studies targeting the catalytic triad, co-enzyme binding site and other amino acid in *D*ADH were used to study *D*ADH function [29-31, 231-236]. If the water relay mechanism is important for the oxidation reaction of *D*ADH, site-directed mutagenesis studies replacing side chains lining the water chain (for example Thr114) would have an effect on the oxidation of substrates and/or destabilize the protein structure by disrupting the internal cavity structure, and effect the kinetic properties of the enzyme. Our collaborators in Spain (Roser Gonzalez-Duarte and Neus Cols) have constructed a mutant *Sl*ADH enzyme where Thr114 has been mutated to Val, (*Sl*ADH^{T114V} mutant) and the X-ray structure of this mutant has been solved by the group of Rudolf Ladenstein in Sweden. Thr114 is lining the eight-membered water channel and mutating Thr114 to Val should break important hydrogen bonds taking part in the putative relay.

The oxidation reaction of *Dm*ADH and *Sl*ADH includes two steps (Figure 2). 1. A proton transfer from the alcohol to the strong base or nucleophile of the binary E•NAD$^+$ complex (the proton transfer step). 2. The hydride transfer from the alcohol to the C4 atom of NAD$^+$ (the hydride transfer step). In both steps, energy is needed in order to

break chemical bonds and facilitate the hydride and proton transfer. However, it is not clear which step takes place first in the oxidation reaction.

Theoretical calculations are important compliments to experimental studies, especially for processes that are impossible or too expensive to study by experimental methods. The QM/MM approach has become a valuable complement to experimental studies for studying chemical reactions involving bond breaking and forming of new bonds. The QM/MM approach contributes with structural insights into such processes. MD methods are valuable approaches for studying molecular motions of importance for ligand binding and molecular mechanics of action of an enzyme.

The specific aims of the present thesis are:

(1) Use enzyme kinetic methods to study the mechanisms of the *Sl*ADH^{T114V} mutant, and compare the results with corresponding studies of wild type (*Sl*ADH^{wt}). In that way we may be able to determine the effect of the mutation on the enzyme kinetic mechanism and thereby the importance of the eight membered water chain for the enzyme kinetics of *Sl*ADH.

(2) Study the effects of the Thr114 to Val mutation on the molecular dynamics of the enzyme by the use of comparative MD simulations of both SlADH^{wt} and SlADH^{T114V} mutant MD simulations of the free enzymes, binary E•NAD$^+$ complexes and ternary E•NAD$^+$•Alcohol complexes should be performed.

(3) Study the proton and hydride transfer of *Sl*ADH using the theoretical QM/MM approach in order to elucidate whether the two steps happen in order.

3 Materials and method

In the following a summary of the methods used in the present thesis is given.

3.1 Experimental studies of the Thr114Val mutant

3.1.1 Determination of kinetic constants of substrates

The oxidation of alcohols and the reduction of acetaldehyde by the *Sl*ADH^{T114V} mutant were studied by steady state kinetics at 23.5 °C. The initial rates were measured by following the appearance and disappearance of NADH, respectively, using a Perkin Elmer λ-16 Spectrophotometer. Buffers used were 0.1 M pyrophosphate (pH 8.5 - 10.0), or 0.1 M phosphate (pH 6.5 - 8.0). The reported aldehyde concentrations represent the sum of the free and hydrated species present.

In all experiments, the Lineweaver-Burk plots obtained were linear within the experimental error. The data fitted equation (1). The unprimed symbols (φ, S) are used for the NAD^+ / alcohol reactions and the primed symbols (φ', S') are used for the NADH / aldehyde reactions. The kinetic coefficients in equation (3) were obtained from primary and secondary plots [237]. The concentrations of coenzyme and substrate used were within the following ranges: NAD^+ 0.24-6.0 mM, ethanol 5-500 mM, propan-2-ol 0.3-40 mM, [$^2H_8$]propan-2-ol 1-40 mM, [$^2H_6$]ethanol 20-500 mM for the alcohol / NAD^+ reactions and NADH 1.5-20 μM, acetaldehyde 0.3-5.0 mM, for the aldehyde / NADH reactions. Inhibition experiments were carried out with either a constant NAD^+ concentration and varied ethanol concentrations, or constant ethanol concentration and varied NAD^+ concentrations.

3.1.2 Active site titration

Due to sample contamination and changing of physical conditions (like freeze drying), a certain proportion of the enzyme may denaturate. During such conditions, the enzyme concentration will be overestimated if it is based on the spectrophotometric method. For the determination of the kinetic coefficients and catalytic properties of an enzyme, it is absolutely necessary to be able to determine the active-enzyme concentration precisely. The best way to do this is to determine the active site concentration of the enzyme by active site titration and relate the obtained enzyme

concentration to a rate assay [103]. Example of this method is spectrophotometric titration [238, 239]. The absorption and difference spectra (Perkin Elmer λ-16 Spectrophotometer) revealed that the formation of the ternary *Sl*ADH^{T114V}•NAD^{+}•Pyrazole complex was accompanied by an absorption peak at 305 nm as previously described for the *Sl*ADH^{wt} and *drosophilid* melanogaster alcohol dehydrogenase (*Dm*ADH) [37, 239, 240]. The mutant *Sl*ADH^{T114V} enzyme containing 100 mM pyrazole was therefore titrated at 305 nm with NAD^{+} in 0.1 M Tris/HCl buffer pH 8.5 at 23.5 °C. The titration experiments were performed in duplicate, with reproducibility within 3 %. The linear parts of the titration curves were analysed by linear regression resulting in regression coefficients better than 0.99. Based on the titrations with the *Sl*ADH^{T114V} mutant enzyme and the assumption that the mutant enzyme has the same ε_{280nm} coefficient as the *Sl*ADH^{wt} enzyme (ε_{280nm} = 13.3 x 10^4 M^{-1} cm^{-1}) [37], it can be concluded that one NAD^{+} molecule was bound to each enzyme subunit. Hence, there are two active sites per enzyme molecule as the enzyme is a dimer.

3.1.3 Rate assay

The rate assay was based on the active site concentrations determined in the titration experiments. The rate assay (performed in duplicate with reproducibility within 5%) was carried out at 23.5°C with a varied concentration of enzyme and a fixed concentration of 1.0 mM of NAD^{+} and 100 mM of ethanol in a total volume of 1 ml of 0.1 M glycine/NaOH buffer, pH 9.5. The velocity v (ΔA_{340nm}/min) is a linear function of [e], the enzyme active site concentration in the cuvette. As $v = k$ [e], a plot of v against [e] gave a rate constant k of 0.192 ($\Delta A_{340nm/min}$ per μN enzyme active sites), with a regression coefficient greater than 0.99. The enzyme concentration is expressed as the amount of subunits in nM. This is twice the amount of enzyme molecules as the enzyme is a dimer.

3.2 Molecular modeling

Most of the graphical interpretation and the RMSD calculation of different enzyme complex were created by using ICM software Version 3.5 (www.molsoft.com). However the molecular modeling calculations like docking, MD simulations, structure optimization, QM/MM calculation were all performed by using the Schrodinger software package [241].

3.2.1 Docking

The X-ray crystal structures of the *Sl*ADH^{wt} (PDB code: 1SBY) and the *Sl*ADH^{T114V} mutant (PDB: 3RJ9) were used as starting structures for computational studies. Both X-ray crystal structures were first optimized with protein preparation wizard in the Maestro V9.1 [242]. Epic [243] was used to model and optimize the three dimensional structures of ethanol and 2-propanol. The 1SBY X-ray crystal structure is a ternary complex containing NAD^+ and the inhibitor 2,2,2-trifluoroethanol, while the *Sl*ADH^{T114V} mutant X-ray structures is a binary E•NAD^+ complex. The 2,2,2-trifluoroethanol molecule from the crystal structure was manually adjusted and optimized to 2-propanol, while ethanol was manually created and optimized. Ethanol and 2-propanol were docked into the active site of both the wild type and mutant using Glide [244]. The best docking poses were selected based on scoring, similarities with the ternary X-ray complex (1SBY) and on the positions of the hydroxyl group and the C_{Alc} atom of the alcohol relative to the $C4_{NAD}$ atom of NAD^+ and the catalytic triad (Ser138, Ty151 and Lys155).

3.2.2 MD simulations

The best docking conformation of 2-propanol and ethanol in both the *Sl*ADH^{wt} and the *Sl*ADH^{T114V} mutant enzymes were selected for MD simulations. The systems were solvated in SPC water molecules in a simulation box of 10Å×10Å×10Å. All the simulations were performed with Desmond [245] for a total of 50 ns (far time step 6fs), using the OPLS-2005 force field [120, 182], under constant pressure of 1 bar and a temperature of 300 K, thermostatted and barostatted using the Nose-Hoover chain [246] and Martyna-Tobias-Klein methods [247]. The short-range and long-range Coulombic interactions were calculated with cutoff (cutoff radius: 9Å) and Smooth particle mesh Ewald [248] methods (Ewald tolerance: 1e-9). All the model systems were relaxed before the simulations using default protocol.

3.2.3 QM/MM calculation

The best docking conformations of ethanol and 2-propanol with the *Sl*ADH^{wt} and the *Sl*ADH^{T114V} mutant were chosen for QM/MM calculation with Qsite [249, 250]. The QM part consisted of (1) the alcohol molecule (2) NAD^+; (3) side chains of Ser138, Tyr151 and Lys155. The side chain oxygen of Tyr151 is believed to act as a strong base

or nucleophile and was therefore negatively charged during the calculations. The four complexes were initially optimized by Qsite and then the QM/MM relaxation scans were performed for two scenarios (the atom labeling is shown in Figure 2):

Scenario 1. The proton (H_{Alc}) transfer from the alcohol donor oxygen (O_{Alc}) to the negatively charged acceptor oxygen on Tyr151 is followed by the hydride (H_{CAlc}) transfer from the donor atom (C_{Alc}) to the NAD^+ acceptor atom ($C4_{NAD}$).

Scenario 2. The hydride transfer from the C_{Alc} to the $C4_{NAD}$ is followed by the proton transfer from O_{Alc} to O^-_{Tyr151}.

Density functional theory (DFT) with the B3LYP function [251] was used for the QM part since this method is particularly useful for studying protein active-site reactive chemistry, while the OPLS-2005 force field [252] was employed for the MM part of the enzyme. The total amount of atoms at QM region was 101. The different atomic bonds were scanned with stepwise increments of 0.02 to 0.052 Å. Non-bonded cut off was not used. It is strongly advised to not use non-bonded cutoff in the QM/MM job settings, because it may create trouble in the optimization and sometimes in the final total energy [253]. The polarization basis sets 631G** [254] was used for all atoms treated quantum mechanically. The QM/MM energy was converted from Hartrees to kcal/mol by using the following interpretation: 627.51 × (QM/MM Energy – lowest QM/MM energy value).

4 Summary of results

4.1 Paper 1

Title: An Intact Eight-Membered Water Chain in Drosophilid Alcohol Short Chain Dehydrogenases/Reductases is Essential for Optimal Enzyme Activity

Pyrazole and 4-bromopyrazole which were ethanol competitive inhibitors with the *Sl*ADH^{T114V} mutant enzyme in the pH region 7.0 to 9.5, showed uncompetitive inhibition against varied NAD^+ concentrations in the same pH region. The *Sl*ADH^{T114V} mutant's oxidation reaction mechanism was consistent with a compulsory ordered mechanism over the entire pH region, where the coenzymes bind to the free enzyme following the substrate binding.

During the oxidation of alcohols, the kinetic coefficients showed that the k_{on} velocity for NAD^+ ($1/\varphi_1$) was approximately 30 times slower for the mutant than for the wild type enzyme over the entire pH region. Furthermore, NAD^+ binds weaker to the mutant than to the wild type enzyme, i.e. the $K_{E,O}$ is larger. The k_{on} velocity for NAD^+ increases with increasing pH for mutant enzyme, which was also observed for the *Sl*ADH^{wt} and slow alloenzymes from *Drosophila melanogaster* (*Dm*ADH^S) [27, 34, 35]. For both the wild type and the mutant, 2-propanol was a better substrate than ethanol. The rate limiting step ($1/\varphi_0$) for ethanol was the hydride transfer step and for 2-propanol enzyme-NADH dissociation step. The kinetic coefficient φ_0 for the oxidation of ethanol and propan-2-ol did not vary within the pH region studied. The hydride transfer step has been reduced by approximately 4 times from $2.4s^{-1}$ in the *Sl*ADH^{wt} enzyme to $0.6s^{-1}$ in the *Sl*ADH^{T114V} mutant. The rate of the enzyme-NADH dissociation step was the same for both mutant and wild type.

The pK_a value of 7.1 ± 0.1 for the wild-type enzyme [34] has been changed to 7.9 ± 0.1 for the mutant. With the *Sl*ADH^{T114V} mutant a primary kinetic isotope effect of 3.5 on φ_0^D / φ_0^H for [$^2H_6$]ethanol and ethanol was obtained.

4.2 Paper 2

Title: Comparative molecular dynamic simulations of wild type and Thr114Val mutated *Scaptodrosophila lebanonensis* alcohol dehydrogenase

MD simulations were performed for the free enzymes, binary E•NAD^+ complexes, ternary enzyme•NAD^+•2propanol (E•NAD^+•2pro) complexes and ternary enzyme•NAD^+•Ethanol (E•NAD^+•Eth) complexes of both the wild type and mutant enzyme.

In the free enzyme simulation: for the *Sl*ADH^{wt}, the RMSD of the backbone stabilized around 2.3-2.7 Å, while the backbone RMSD of the *Sl*ADH^{T114V} mutant varied between 2.1 and 2.9 Å (Figure 1 in paper2). Compared with Thr114 in the wild type, Val114 in the mutant is lacking a hydroxyl group and only a hydrogen bond between backbone NH of Val114 and the backbone CO group of Gly 110 was seen. This hydrogen bond was also maintained during the entire 50 ns of MD.

In the wild type E•NAD^+ binary complex, the adenine part of NAD^+ formed hydrogen bonds with Asp63 and Val64 that persisted during the entire 50 ns of MD, while these hydrogen bonds were broken after around 4 ns in mutant and were not seen for the rest of the MD. The nicotinamide part of NAD^+ formed a hydrogen bond to Thr186 during MD of both the wild type and mutant binary complex. The hydrogen bond seemed more persistent during MD with the mutant binary complex than during MD with the wild type binary complex. In the region of amino acid 114 (mutation region), Gly110 interacted mainly with Thr114 by forming two hydrogen bonds in wild type. In the mutant, Gly110 interacted with Asn113 and the back bond NH group of Val114. RMSF profile showed reduced fluctuation of the region around amino acids 175 -195 that is located on the protein surface being important for binding the nicotinamide part of NAD^+ during MD with the mutant compared with that of the wild type (Figure 4 in paper2).

In the E•NAD^+•2pro complex, the hydrogen bonds between the adenine part of NAD^+ and Asp63/Val64 were stable during MD with the wild type, while in the mutant, these interactions were gradually reduced. For the wild type the RMSD for NAD^+ was between 0.0 Å to 2.0 Å, while for the mutant the RMSD for NAD^+ was between 0.5 Å to 2.5Å. The side chain carbon atoms of the hydrophobic amino acids Ile106 and Val64 were closer to each other in the *Sl*ADH^{T114V} mutant than in the *Sl*ADH^{wt}. In the wild type

the atomic distance between their closest side chain carbon atoms was continuously 6 Å, while the corresponding distance in the mutant was 6 Å during the first 10 ns, then it dropped to around 4.5 Å for the rest of the simulation. Both the side chain OH group and the backbone NH group of Ser71 formed very stable hydrogen bonds with Pro67, while in the wild type, only the backbone NH group interacted stably with Pro67, while the side chain was in the direction of Tyr62 altering the position of Tyr62 compared with the mutant. The interaction between Gly110 and Thr114 in the wild type remained the stable during the entire 50 ns of MD, while in the mutant, Gly110 interacted not only with Val114 backbone -NH group, but also with Asn90 and a water molecule during MD.

After 12 ns of simulation with the ternary E•NAD^+•Eth complex of the mutant, the hydrogen bonds between the adenine part and Asp63 and Val64 were broken, while the hydrogen bond between nicotinamide part and Thr186 was not observed between 10 and 20 ns, but were for the rest of the simulation. Calculations of the RMSD of NAD^+ during MD of the mutant showed an increase from 0.5 Å to 2.5 Å during the first 7 ns, for the rest of the MD the RMSD was stable between 2.5~3.5Å. In the wild type, the interactions of the nicotinamide part of NAD^+ with Thr186 and the interactions of the adenine part with Asp63 and Val64 were stable during the entire 50 ns of simulation. The side chain atomic distances Ala92 - Val64 and Ile106 - Val64 were quite stable during MD with the wild type ternary complex, while during MD with the mutant these distances increased from 4 to 8 Å (Ala92-Val64) and from 6 to 10 Å (Ile106-Val64). Gly110 in the mutant interacted with Asn90 during the first 30 ns, and then changed to the backbone NH group of Val114. During MD with the wild type, Gly110 mainly interacted with Thr114.

The catalytic triad (Ser138, Tyr151 and Lys155) remained quite stable in both wild type and mutant free enzyme.

4.3 Paper 3

Title: QM/MM studies of the catalytic mechanism of short chain alcohol dehydrogenases

After docking, the H_{Alc} (Figure 2) of both 2-propanol and ethanol was located at a distance of 1.59 Å from the O^{-}_{Tyr151} atom in the wild type. In the ternary *Sl*ADH^{T114V} mutant complexes, the H_{Alc} of both 2-propranol and ethanol was located around 1.50 Å from the O^{-}_{Tyr151} atom.

In scenario 1a (Figure 2 in paper 3) , QM/MM energies for E•NAD^{+}•2pro wild type complex increased by approximately 7 kcal/mol when going from the energy optimized complex until the complex with the H_{Alc}–O^{-}_{Tyr151} atomic distance of 0.95 Å was obtained. During the successive decrease of the H_{Alc}–O^{-}_{Tyr151} atom distance, the C_{Alc}–O_{Alc} atomic distance decreased automatically from 1.44 to 1.40 Å. However, the C_{Alc}–H_{CAlc} and H_{CAlc}–$C4_{NAD}$ atomic distances did not change. The energy developments during the relaxation scan 1b for 2-propanol indicated that activation energy of about 20 kcal/mol was needed, then the energy drops with approximately 17 kcal/mol until a stable H_{CAlc} – $C4_{NAD}$ atomic distance of 1.10 Å was formed.

In scenario 2a (Figure 2 in paper 3), at an H_{CAlc} –$C4_{NAD}$ atomic distance of 1.095 Å the QM/MM energy reached minimum. Between increment step 18 and 19 of 2-propanol with the wild type enzyme, the H_{CAlc}–$C4_{NAD}$ atomic distance changed from 1.47 to 1.42 Å, but the H_{Alc}–O^{-}_{Tyr151} distance changed from 1.43 Å (increment 18) to 1.029 Å (increment 19), while C_{Alc}–O_{Alc} changed dramatically from 1.39 to 1.32 Å and the O_{Alc}–H_{Alc} atomic distance changed from 1.067 Å to 1.52 Å (Figure 5 and 6 in paper 3). Similar sudden changes in the region of the alcohol hydroxyl group were also observed during the H_{CAlc}–$C4_{NAD}$ distance relaxation scan of other wild type and mutant ternary complexes. At the end of the relaxation scans when the QM/MM energy had reached the energy minimum, at a H_{CAlc}–$C4_{NAD}$ atomic distance of 1.095 Å, the H_{Alc}–O^{-}_{Tyr151} distances were: wild type E•NAD^{+}•2pro complex: 0.98 Å, the wild type E•NAD^{+}•Eth complex: 0.98 Å, the mutant E•NAD^{+}•2pro complex 0.99 Å and the mutant E•NAD^{+}•Eth complex 0.97 Å (Figure 4 in paper 3). During the relaxation scan the C_{Alc}–O_{Alc} changed into a double bond in all calculations with an atomic distance around 1.23Å. The

calculations indicated that a double bond character was induced into C_{Alc}–O_{Alc} bond before the H_{CAlc}–$C4_{NAD}$ relaxation scan was ended. For the ternary complex of E•NAD^+•2pro with the wild type enzyme, a C_{Alc}–O_{Alc} double bond was formed between increment steps 19 to 23. During these steps, the C_{Alc}–O_{Alc} bond distance change from 1.33 Å to 1.24 Å, while H_{CAlc}–$C4_{NAD}$ bond distance changed from 1.42 Å to 1.21 Å, while the hydride transfer relaxation was continued until an H_{CAlc}–$C4_{NAD}$ atomic distance of 1.105 Å at increment step 25. A similar change in the hydride transfer was not observed during the relaxation scan of the scenario (Figure 3 in paper 3).

5 Discussion

The SDR family is the best studied family of the ADHs, and several review papers have covered this group of enzymes during the last years [8, 10, 62, 255-257]. With the fast development of genome projects, the number of identified SDR primary sequences has increased from around 2000 [255] to around 47000 [8] during the last ten years. These primary sequences come from a variety of different species. A web site based on SDR related research has also been constructed (http://www.sdr-enzymes.org/).

In humans there are, so fare, 202 SDR forms, among which 24 enzymes are associated with diseases in the OMIM database (Online Mendelian Inheritance in Man) [8]. However, the functions of about half of the human SDR enzymes are unknown [8]. Therefore, understanding the function and chemical reaction mechanism of SDR is also medically very important. Studies from different species have indicated that most enzymes in the SDR family have large similarities in the active site architecture (Figure 4), and are either NAD^+ or $NADP^+$ specific or utilize both coenzymes [8, 10, 62, 255-257]. Based on these similarities it is reasonable to believe that SDRs from *drosophilid* species may be used as a model system for other enzymes in the SDR family.

SDRs from *drosophilid* species are among the most convenient to study. In these SDRs the nucleotides stereospecifically transfers a hydride from or to a substrate carbon atom and position 4 of the nicotinamide ring, and a lot is known about their molecular mechanism of action. However, the exact mechanism is still unknown. A chain of eight water molecules that is conserved in all *D*ADHs has been proposed to be involved in a proton relay mechanism transporting a proton in between the active site and the solvent [19, 20, 46]. In the present study, the *Sl*ADH^{T114V} mutant was studied by experimental enzyme kinetic studies and theoretical molecular modeling studies, while the *Sl*ADH^{wt} was studied by theoretical molecular modeling studies. The main focus was on the function of this water chain and on the proton transfer and hydride transfer steps during the oxidation of *Sl*ADH.

5.1 The eight membered water chain in DADHs

5.1.1 Enzyme Kinetic studies of SlADHT114V

Highly pure preparations of *Sl*ADH^{T114V} mutant were obtained from one of our collaborators. The proton relay chain in the *Sl*ADH^{wt} is shown in Figure 3. The resolved X-ray crystal structure of the SlADH^{T114V} mutant (Figure 13) shows high similarity to the structure of the wild-type enzyme (Figure 3), although the eight-membered water chain in the SlADH^{T114V} mutant is interrupted by the lack of the hydroxyl group at the side chain in position 114. However, differences in the kinetic properties between *Sl*ADH^{wt} and *Sl*ADH^{T114V} were found.

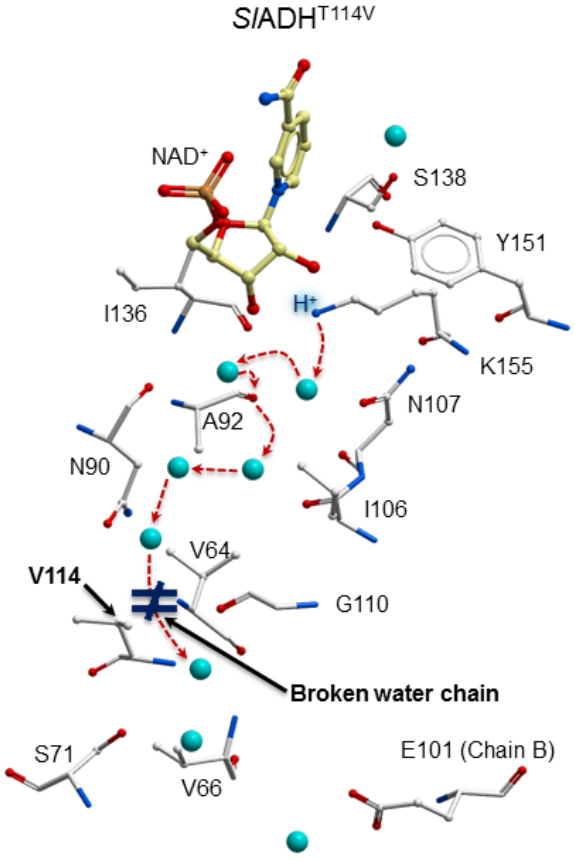

Figure 13: Eight membered water chain in X-ray crystal structure of SlADH^{T114V} mutant (PDB Code: 3RJ9).

Pyrazole and 4-bromopyrazole which were ethanol competitive inhibitors with the *Sl*ADH^{T114V} mutant enzyme in the pH region 7.0 to 9.5, showed uncompetitive inhibition against varied NAD^+ in the same pH region, and not mixed inhibition pattern. Therefore, like the wild type [19, 21, 33, 37, 54, 230], binding of coenzyme and substrate to the *Sl*ADH^{T114V} mutant is also consistent with a compulsory ordered reaction mechanism

(Scheme 2, Figure 6) with the coenzyme binding to the free enzyme before the substrate binding. This is valid for the entire pH region studied. This was further proved by the independency of φ_1 coefficient (the binding of NAD^+ to the free enzyme) at both pH 7.0 and 9.5 with different alcohols.

With the *Sl*ADH^{T114V} mutant a primary kinetic isotope effect of 3.5 on $\varphi_0{}^D$ / $\varphi_0{}^H$ for [$^2H_6$]ethanol and ethanol was obtained. This is of the same magnitude as previously obtained for the *Sl*ADH^{wt} enzyme and the *Drosophila melanogaster* alleloenzymes ADH^S, ADH^F and ADH^{UF} [34, 36, 37, 258, 259]. This primary kinetic isotope effect indicates that the interconversion of the ternary complexes, i.e. the hydride transfer step (*k*) largely contributes to the rate limiting step in the oxidation of ethanol. The hydride transfer step has been reduced by approximately 4 times from 2.4s^{-1} in the *Sl*ADH^{wt} enzyme to 0.6s^{-1} in the *Sl*ADH^{T114V} mutant. As with the wild-type enzyme, the rate of the hydride transfer step for ethanol with the mutant enzyme does not vary with pH.

For the *Sl*ADH^{wt} enzyme and the various *Dm*ADH alleloenzymes, the hydride transfer rate (*k*) for the secondary alcohol propan-2-ol was large compared to the E•NADH dissociation step (k'_{-1}) [34, 35]. The reduction in hydride transfer rate introduced by a deuterium atom did not affect the maximum velocity. For the *Sl*ADH^{T114V} mutant, the E•NADH dissociation rate (k'_{-1}) was approximately the same as for the wild-type enzyme. The small primary isotope effect ($\varphi_0{}^D$ / $\varphi_0{}^H$) of approximately 1.6 obtained for [$^2H_8$]propan-2-ol in relation to propan-2-ol reveals that the rate limiting step with the isotope labelled alcohol has been changed to also include the hydride transfer step in addition to the E•NADH dissociation step. This also suggests that the rate of the hydride transfer step with propan-2-ol as a substrate has been reduced in the mutant compared to the wild-type enzyme.

Previous studies with the *Sl*ADH^{wt} and the *Dm*ADH^S showed that the pH dependence of the alcohol binding to the binary E·NAD^+ complex is derived exclusively from the on-velocity constant k_2 [27, 34, 43]. The present work with the *Sl*ADH^{T114V} mutant showed that the binding of ethanol to the binary *D*ADH•NAD^+ complex also is dependent on the release of a single proton from the binary complex and that the hydride transfer step is pH independent. The 0.8 unit increase in the pK_a value for binding of ethanol to the mutant *D*ADH•NAD^+ complex compared to the wild type complex

supports the water relay hypothesis of a linked ionization of the Tyr151/Lys155 residues in the active site. The orientation of the Thr114 OH group is pH dependent. Hence, Thr114 can be considered as a switch that keeps the water chain active, i.e. acting as proton relay. The change of Thr114 to Val114 in the mutant results in a break of the hydrogen bond pattern in the water chain (Figure 13), and hence affects the proton release to the bulk water through the water chain. Thus our results suggest that the water channel in *D*ADH acts as a proton relay in the binary *D*ADH•NAD^+ complex. However, our results reveal the hydride transfer step in the mutant enzyme is 4 times slower than in the wild-type enzyme. This suggests that the water chain also is important for the hydride transfer and that the proton transfer may affect the rate of the hydride transfer.

5.1.2 Molecular dynamic perspective of $SlADH^{wt}$ and $SlADH^{T114V}$

From enzyme kinetic perspective, the studies in paper 1 verified the compulsory ordered mechanism of the *Sl*ADH^{T114V} mutant and that the water relay system is important for optimal oxidation of alcohols by *Sl*ADH^{wt}. However, in spite of differences in the enzyme kinetic constants, the X-ray crystal structure of the $SlADH^{T114V}$ mutant was very similar to the structure of *Sl*ADH^{wt}. The important question in paper 2 was therefore if the Thr114 to Val mutation not only could interfere with the proton relay system by removing a connecting link in the chain, but also induce differences in molecular dynamics between the *Sl*ADH^{wt} and the *Sl*ADH^{T114V} mutant. Molecular motions are important for proper enzyme function, and differences in the structural dynamics between the *Sl*ADH^{wt} and the *Sl*ADH^{T114V} mutant may also contribute to the differences in their kinetic coefficients. The molecular dynamics simulations in paper 2 showed that there were differences in molecular dynamics in different regions of the enzymes between the *Sl*ADH^{wt} and the *Sl*ADH^{T114V} mutant.

Measuring the substrate H_{Alc}–O^-_{Tyr151} and H_{CAlc}–$C4_{NAD}$ atomic distances during the MD showed that both 2-propanol and ethanol had more freedom for movements in the active site region of the *Sl*ADH^{wt} than of the *Sl*ADH^{T114V} mutant. This may in part explain the faster hydride transfer rate in the wild type enzyme compared to the mutant enzyme. In this region, the hydrogen bonding between Thr186 and nicotinamide ring of NAD^+ is important for NAD^+ binding. This hydrogen bond was stable in MD of the wild type ternary complexes. While in the mutant ternary complex, this hydrogen bond was

broken. However, during MD of the binary complexes, this hydrogen bond was more often seen in the mutant. This may indicate that substrate binding is favourable for forming the hydrogen bond between Thr186 and NAD^+. The simulations indicated that the Thr114 to Val mutations alters the hydrogen bonding interactions between Thr186 and the nicotinamide ring of NAD^+ and thereby induces differences in the dynamical behaviour in the region of amino acids 175-210.

Hydrophobic interaction and hydrogen bonds are the two main types of interaction between the adenine part of NAD^+ and the hydrophobic pocket. The hydrogen bonding of adenine to both Asp63 and Val64 were generally reduced during MD with the mutant binary and ternary complexes compared with the corresponding wild type complexes. The adenine ring of NAD^+ was then twisted closer to the water channel in the mutant than in the wild type.

Another consequence of this change was the increased atomic distances between the side chain atoms of Ala92 and Val64 and between the side chain atoms of Ile106 and Val64 during the simulations of the ternary complexes of ethanol with the *Sl*ADH^{T114V} mutant, while the atomic distance between Ile106 and Val64 decreased during MD of the ternary complex of 2-propanol with the *Sl*ADH^{T114V} mutant. However, during all simulations with the ternary complexes of the *Sl*ADH^{wt}, these atomic distances remained stable. These differences observed during the MD in the region of the adenine and nicotinamide moiety of NAD^+ between the *Sl*ADH^{wt} and the *Sl*ADH^{T114V} mutant may affect the NAD^+ binding at Rossman fold and contribute to the experimentally observed differences in NAD^+ dissociation constant. The eight membered water channel may also be influenced by these dynamical changes since the water channels is situated close to the Rossman fold and the altered dynamics in the *Sl*ADH^{T114V} mutant due to the mutation may therefore also affect the proton abstraction from the binary enzyme-NAD^+ complex.

Another hot spot is the region around amino acid 114. Several amino acids such as Gly110, Tyr62, Ser71, Pro67, Asn113 and Val66 are located around Thr144 (Val114). These amino acids may facilitate the proton transport from the NH_3-group at the side chain of Lys155 into the bulk solution through the end part of water channel [260]. In the wild type enzyme, the MDs of the *Sl*ADH^{T114V} indicated that several intramolecular interactions in this area disappeared or were reduced due to the Thr to Val mutation. An

interaction between Tyr62 and Ser71 seems very important since it is located in the end part of proton relay system close to the bulk solution (Figure 3). This interaction was also reduced during MD with the *Sl*ADH^{T114V} enzyme complexes and of the free *Sl*ADH^{T114V} mutant enzyme compared with the corresponding simulations of the *Sl*ADH^{wt}. All these differences in bonding interactions observed during MDs of the *Sl*ADH^{T114V} mutant compared to the MDs of the *Sl*ADH^{wt} in the region of water channel may contribute to a destabilizing of the end section of water chain in the mutant.

5.1.3 QM/MM studies of oxidation reaction mechanism of SlADH

In paper 1 we mentioned the relationship between water relay system and the two steps in alcohol oxidation reaction (hydride transfer and proton release). The experimental result indicated that the hydride transfer step in the oxidation of ethanol was approximately 4 times slower for the *Sl*ADH^{T114V} mutant than for the *Sl*ADH^{wt}. One can anticipate that disruption caused by the Thr114 to Val mutation on the water chain may affect the hydride transfer step under certain conditions. It is obvious that the differences in molecular motions between the *Sl*ADH^{T114V} mutant and the *Sl*ADH^{wt} found in paper 2 may contribute to the difference in hydride transfer. However, other differences may also contribute that can depend on whether the proton transfer occurs prior to or at the same time as the hydride transfer and alternatively regulate the latter step. In paper 3 we were using QM/MM calculations to study the proton and hydride transfer steps during alcohol oxidation of both the *Sl*ADH^{wt} and the *Sl*ADH^{T114V} mutant enzymes. Labeling of atoms mentioned in this section is given in Figure 2.

Previous studies have suggested that proton abstraction from the hydroxyl group of alcohol is drawn by a negatively charged Tyr151 that may be also be coupled to Lys155 [33, 46, 54, 230]. After docking and energy optimization of the ternary *Sl*ADH^{T114V} mutant and *Sl*ADH^{wt} complexes, the hydroxyl hydrogen atoms (H_{Alc}) of both 2-propanol and ethanol were located much closer to Tyr151 (approximately 1.6Å) than to Lys155 (approximately 4Å). This may indicate that the proton most likely is donated to Tyr151.

During the QM/MM calculations of the hydride transfer step it seemed like the proton transfer step was closely linked to the hydride transfer step. When the C_{Alc}–H_{CAlc} atomic distance (Figure 2) has increased to 1.275 Å and the H_{CAlc}–$C4_{NAD}$ atomic distance

(Figure 2) has decreased to 1.415 Å. we also got a sudden change in the C_{Alc}–O_{Alc} atom distance (1.43Å→1.32Å) and in the H_{Alc}–O^{-}_{Tyr151} atomic distances (1.57Å→1.03Å) indicating that the proton transfer was initiated by the hydride transfer. Similar results were also obtained during the QM/MM relaxtion scans of the other complexes, the ternary complex of the *Sl*ADH^{wt} with ethanol and the ternary complexes of the *Sl*ADH^{T114v} mutant with 2-propanol and ethanol. This indicates three interesting phenomena: (1) Hydride transfer starts and at some point during the course, proton transfer starts and finish. (2) At the point when the proton transfer starts, a partly double bond character has been induced into the C_{Alc}–O_{Alc} bond. (3) The hydride transfer continues until reaching its finishing point accompanied with the formation of a C_{Alc}–O_{Alc} double bond.

Especially, forming the partly double bond character most likely affects the pK_a value of the alcohol OH group to a value lower than 7.1, i.e. the pK_a value of the Tyr/Lys couple at the catalytic site of the wild type enzyme. This may explain why H_{Alc} is transferred to O^{-}_{Tyr151}.

However during QM/MM calculation of the scenario in which the proton transfer happens prior to hydride transfer step, the C_{Alc}–O_{Alc} atomic distance was only slightly decreased (from 1.44 Å to 1.4 Å) and a double bond character was not induced. Calculation of the activation energy for our favorable scenario showed that the *Sl*ADH^{wt} had lower activation energy than the *Sl*ADH^{T114V} mutant for 2-propanol, while the activation energy was highest for the *Sl*ADH^{wt} with ethanol. That may indicate that the activation energy is not the reason for slower hydride transfer for the *Sl*ADH^{T114V} mutant compared with the *Sl*ADH^{wt}.

6 Conclusion

Despite their highly diverse substrate specificities, SDR family members show very similar folding pattern architectures, suggesting similarities in the catalytic mechanism and hence that *Sl*ADH can be used as a model enzyme for other SDR enzymes. The present study showed that the introduction of a Val instead of a Thr at position 114 in *Sl*ADH results in a break of the proton relay system. This break results in a slower k_{on} velocity of NAD^+ and a weaker binding of this coenzyme to the enzyme. Furthermore, it results in a slower hydride transfer from alcohol to NAD^+ and an increase the pK_a value of the group in the binary enzyme•NAD^+ complex that regulates the k_{on} velocity of the alcohol and alcohol competitive inhibitors. Hence, an intact water chain in *drosophilid* ADHs is essential for optimal enzyme activity. Other factors may also contribute to these changes, such as an altered dynamical behavior due to the mutation and the broken water chain.

During the alcohol oxidation, hydride transfer most likely start first and initiate the proton transfer by lowering the pK_a of hydroxyl group on alcohol. When the proton transfer is finished, the hydride transfer continues until it is finished. However, it is also important to have in mind the QM/MM method used in the present study has limitations, and the calculated activation energies could not explain why the hydride transfer is slower in the *Sl*ADH^{T114V} mutant than in the *Sl*ADH^{wt}, but still gives complementary explanations to the reaction order of these two steps. More experimental and theoretical studies are necessary in order to gain more insight into the proton relay mechanism and the alcohol oxidation mechanism of *Sl*ADH.

7 Reference

1. Winberg, J.O., et al., *Kinetic interpretations of active site topologies and residue exchanges in Drosophila alcohol dehydrogenases.* Int J Biochem, 1992. **24**(2): p. 169-81.
2. Kavanagh, K.L., et al., *Medium- and short-chain dehydrogenase/reductase gene and protein families : the SDR superfamily: functional and structural diversity within a family of metabolic and regulatory enzymes.* Cell Mol Life Sci, 2008. **65**(24): p. 3895-906.
3. Persson, B., et al., *Medium- and short-chain dehydrogenase/reductase gene and protein families : the MDR superfamily.* Cell Mol Life Sci, 2008. **65**(24): p. 3879-94.
4. Lee, T., *Characterization of fatty alcohol:NAD+ oxidoreductase from rat liver.* J Biol Chem, 1979. **254**(8): p. 2892-6.
5. Klimacek, M., et al., *A catalytic consensus motif for D-mannitol 2-dehydrogenase, a member of a polyol-specific long-chain dehydrogenase family, revealed by kinetic characterization of site-directed mutants of the enzyme from Pseudomonas fluorescens.* Biochemical Journal, 2002. **367**: p. 13-18.
6. Jornvall, H., et al., *SDR and MDR: completed genome sequences show these protein families to be large, of old origin, and of complex nature.* FEBS Lett, 1999. **445**(2-3): p. 261-4.
7. Pearl, F., et al., *The CATH Domain Structure Database and related resources Gene3D and DHS provide comprehensive domain family information for genome analysis.* Nucleic Acids Res, 2005. **33**(Database issue): p. D247-51.
8. Kallberg, Y., et al., *Classification of the short-chain dehydrogenase/reductase superfamily using hidden Markov models.* FEBS J, 2010. **277**(10): p. 2375-86.
9. Jornvall, H., et al., *Short-chain dehydrogenases/reductases (SDR).* Biochemistry, 1995. **34**(18): p. 6003-13.
10. Ladenstein, R., et al., *Medium- and short-chain dehydrogenase/reductase gene and protein families : Structure-function relationships in short-chain alcohol dehydrogenases.* Cell Mol Life Sci, 2008. **65**(24): p. 3918-35.
11. Shi, R., et al., *Cofactor hydrogen bonding onto the protein main chain is conserved in the short chain dehydrogenase/reductase family and contributes to nicotinamide orientation.* J Biol Chem, 2004. **279**(16): p. 16778-85.
12. Oppermann, U.C., et al., *Forms and functions of human SDR enzymes.* Chem Biol Interact, 2001. **130-132**(1-3): p. 699-705.
13. Azzouni, F., et al., *The 5 alpha-reductase isozyme family: a review of basic biology and their role in human diseases.* Adv Urol, 2012. **2012**: p. 530121.
14. Fomitcheva, J., et al., *Characterization of Ke 6, a new 17beta-hydroxysteroid dehydrogenase, and its expression in gonadal tissues.* J Biol Chem, 1998. **273**(35): p. 22664-71.
15. Lin, S.X., et al., *3D-structure of human estrogenic 17beta-HSD1: binding with various steroids.* J Steroid Biochem Mol Biol, 1999. **69**(1-6): p. 425-9.

16. He, X.Y., et al., *Human brain short chain L-3-hydroxyacyl coenzyme A dehydrogenase is a single-domain multifunctional enzyme. Characterization of a novel 17beta-hydroxysteroid dehydrogenase.* J Biol Chem, 1999. **274**(21): p. 15014-9.
17. Masuzaki, H., et al., *A transgenic model of visceral obesity and the metabolic syndrome.* Science, 2001. **294**(5549): p. 2166-70.
18. Berman, H.M., et al., *The Protein Data Bank.* Nucleic Acids Res, 2000. **28**(1): p. 235-42.
19. Benach, J., et al., *The refined crystal structure of Drosophila lebanonensis alcohol dehydrogenase at 1.9 A resolution.* J Mol Biol, 1998. **282**(2): p. 383-99.
20. Benach, J., et al., *The catalytic reaction and inhibition mechanism of Drosophila alcohol dehydrogenase: observation of an enzyme-bound NAD-ketone adduct at 1.4 A resolution by X-ray crystallography.* J Mol Biol, 1999. **289**(2): p. 335-55.
21. Benach, J., Meijers, R., Atrian, S., Gonzalez-Duarte, R., Lamzin, V.S., Ladenstein, R, *1.1-Å crystal structure of D. lebanonensis ADH complexed with NAD+ and 2,2,2-trifluoroethanol.* PDB database, 2005.
22. Benach, J., et al., *Drosophila alcohol dehydrogenase: acetate-enzyme interactions and novel insights into the effects of electrostatics on catalysis.* J Mol Biol, 2005. **345**(3): p. 579-98.
23. Morgunova, E., Wuxiuer, Y., Cols, N., Popov, A., Sylte, I., Karshikoff, A., Gonzales-Duarte, R., Ladenstein, R., Winberg, J.O, *Structure of alcohol dehydrogenase from Drosophila lebanonesis T114V mutant complexed with NAD+*. In press, 2012.
24. Oppermann, U., et al., *Short-chain dehydrogenases/reductases (SDR): the 2002 update.* Chem Biol Interact, 2003. **143-144**: p. 247-53.
25. Benach, J., et al., *Structure-function relationships in Drosophila melanogaster alcohol dehydrogenase allozymes ADH(S), ADH(F) and ADH(UF), and distantly related forms.* Eur J Biochem, 2000. **267**(12): p. 3613-22.
26. Oppermann, U.C., et al., *Molecular and structural aspects of xenobiotic carbonyl metabolizing enzymes. Role of reductases and dehydrogenases in xenobiotic phase I reactions.* Toxicology, 2000. **144**(1-3): p. 71-81.
27. Winberg, J.O., et al., *The catalytic triad in Drosophila alcohol dehydrogenase: pH, temperature and molecular modelling studies.* J Mol Biol, 1999. **294**(2): p. 601-16.
28. Albalat, R., et al., *Protein engineering of Drosophila alcohol dehydrogenase. The hydroxyl group of Tyr152 is involved in the active site of the enzyme.* FEBS Lett, 1992. **308**(3): p. 235-9.
29. Chen, Z., et al., *Site-specific mutagenesis of Drosophila alcohol dehydrogenase: evidence for involvement of tyrosine-152 and lysine-156 in catalysis.* Biochemistry, 1993. **32**(13): p. 3342-6.
30. Cols, N., et al., *Drosophila alcohol dehydrogenase: evaluation of Ser139 site-directed mutants.* FEBS Lett, 1997. **413**(2): p. 191-3.
31. Cols, N., et al., *Effect of site-directed mutagenesis on conserved positions of Drosophila alcohol dehydrogenase.* FEBS Lett, 1993. **319**(1-2): p. 90-4.
32. Lin, Z.G., et al., *Serine 139 of Drosophila alcohol dehydrogenase is an essential residue for activity.* FASEB J, 1993. **7**(7): p. A1196.

33. Brendskag, M.K., et al., *Drosophila lebanonensis alcohol dehydrogenase: pH dependence of the kinetic coefficients.* Biochimica Et Biophysica Acta-Protein Structure and Molecular Enzymology, 1999. **1431**(1): p. 74-86.
34. Brendskag, M.K., et al., *Drosophila lebanonensis alcohol dehydrogenase: pH dependence of the kinetic coefficients.* Biochim Biophys Acta, 1999. **1431**: p. 74-86.
35. Winberg, J.O., et al., *The AdhS alleloenzyme of alcohol dehydrogenase from Drosophila melanogaster. Variation of kinetic parameters with pH.* Biochem J, 1988. **255**(2): p. 589-99.
36. Winberg, J.O., et al., *Alcohol dehydrogenase from the fruitfly Drosophila melanogaster. Substrate specificity of the alleloenzymes AdhS and AdhUF.* Biochim Biophys Acta, 1982. **704**(1): p. 7-16.
37. Winberg, J.O., et al., *Biochemical properties of alcohol dehydrogenase from Drosophila lebanonensis.* Biochem J, 1986. **235**(2): p. 481-90.
38. Hovik, R., et al., *Drosophila-Melanogaster Alcohol-Dehydrogenase - Substrate Stereospecificity of the Adhf Alleloenzyme.* Insect Biochemistry, 1984. **14**(3): p. 345-351.
39. Chambers, G.K., *The Drosophila Alcohol-Dehydrogenase Gene-Enzyme System - Introduction.* Advances in Genetics Incorporating Molecular Genetic Medicine, 1988. **25**: p. 40-107.
40. Chambers, G.K., *Gene-Expression, Adaptation and Evolution in Higher Organisms - Evidence from Studies of Drosophila Alcohol Dehydrogenases.* Comparative Biochemistry and Physiology B-Biochemistry & Molecular Biology, 1991. **99**(4): p. 723-730.
41. Gani, O.A., et al., *Theoretical calculations of the catalytic triad in short-chain alcohol dehydrogenases/reductases.* Biophys J, 2008. **94**(4): p. 1412-27.
42. Ghosh, D., et al., *The refined three-dimensional structure of 3 alpha,20 beta-hydroxysteroid dehydrogenase and possible roles of the residues conserved in short-chain dehydrogenases.* Structure, 1994. **2**(7): p. 629-40.
43. McKinley-McKee, J.S., et al., *Mechanism of action of Drosophila melanogaster alcohol dehydrogenase.* Biochem Int, 1991. **25**(5): p. 879-85.
44. Tanaka, N., et al., *Crystal structures of the binary and ternary complexes of 7 alpha- hydroxysteroid dehydrogenase from Escherichia coli.* Biochemistry, 1996. **35**(24): p. 7715-30.
45. Tanabe, T., et al., *Roles of the Ser146, Tyr159, and Lys163 residues in the catalytic action of 7alpha-hydroxysteroid dehydrogenase from Escherichia coli.* J Biochem, 1998. **124**(3): p. 634-41.
46. Koumanov, A., et al., *The catalytic mechanism of Drosophila alcohol dehydrogenase: evidence for a proton relay modulated by the coupled ionization of the active site Lysine/Tyrosine pair and a NAD+ ribose OH switch.* Proteins, 2003. **51**(2): p. 289-98.
47. Williams, M.A., et al., *Buried waters and internal cavities in monomeric proteins.* Protein Sci, 1994. **3**(8): p. 1224-35.
48. Renthal, R., *Buried water molecules in helical transmembrane proteins.* Biophysical Journal, 2007: p. 74a-74a.

49. Raschke, T.M., *Water structure and interactions with protein surfaces.* Current Opinion in Structural Biology, 2006. **16**(2): p. 152-159.
50. Park, S., et al., *Statistical and molecular dynamics studies of buried waters in globular proteins.* Proteins: Structure, Function, and Bioinformatics, 2005. **60**(3): p. 450-463.
51. Carugo, O., et al., *How many water molecules can be detected by protein crystallography?* Acta Crystallographica Section D, 1999. **55**(2): p. 479-483.
52. Winberg, J.O., et al., *Drosophila melanogaster alcohol dehydrogenase. Biochemical properties of the NAD+-plus-acetone-induced isoenzyme conversion.* Biochem J, 1988. **251**(1): p. 223-7.
53. Winberg, J.O., et al., *Drosophila melanogaster alcohol dehydrogenase: mechanism of aldehyde oxidation and dismutation.* Biochem J, 1998. **329 (Pt 3)**: p. 561-70.
54. Winberg, J.O., et al., *The catalytic triad in Drosophila alcohol dehydrogenase: pH, temperature and molecular modelling studies.* Journal of Molecular Biology, 1999. **294**(2): p. 601-616.
55. El-Kabbani, O., et al., *Crystal structure of human L-xylulose reductase holoenzyme: probing the role of Asn107 with site-directed mutagenesis.* Proteins, 2004. **55**(3): p. 724-32.
56. Filling, C., et al., *Critical residues for structure and catalysis in short-chain dehydrogenases/reductases.* J Biol Chem, 2002. **277**(28): p. 25677-84.
57. Kubota, K., et al., *The crystal structure of l-sorbose reductase from Gluconobacter frateurii complexed with NADPH and l-sorbose.* Journal of molecular biology, 2011. **407**(4): p. 543-55.
58. Gramser, S., *Alcohol and science: the party gene.* Nature, 2005. **438**(7071): p. 1068-9.
59. Ashburner, M., *Speculations on the subject of alcohol dehydrogenase and its properties in Drosophila and other flies.* Bioessays, 1998. **20**(11): p. 949-54.
60. Whitworth, A.J., et al., *Drosophila models pioneer a new approach to drug discovery for Parkinson's disease.* Drug Discov Today, 2006. **11**(3-4): p. 119-26.
61. Hopkins, A.L., et al., *The druggable genome.* Nat Rev Drug Discov, 2002. **1**(9): p. 727-30.
62. Persson, B., et al., *The SDR (short-chain dehydrogenase/reductase and related enzymes) nomenclature initiative.* Chem Biol Interact, 2009. **178**(1-3): p. 94-8.
63. Bray, J.E., et al., *The human short-chain dehydrogenase/reductase (SDR) superfamily: a bioinformatics summary.* Chem Biol Interact, 2009. **178**(1-3): p. 99-109.
64. Day, J.M., et al., *Design and validation of specific inhibitors of 17beta-hydroxysteroid dehydrogenases for therapeutic application in breast and prostate cancer, and in endometriosis.* Endocr Relat Cancer, 2008. **15**(3): p. 665-92.
65. Jemal, A., et al., *Global cancer statistics.* CA Cancer J Clin, 2011. **61**(2): p. 69-90.
66. Bulun, S.E., et al., *Estrogen biosynthesis in endometriosis: molecular basis and clinical relevance.* J Mol Endocrinol, 2000. **25**(1): p. 35-42.
67. Day, J.M., et al., *17beta-hydroxysteroid dehydrogenase Type 1, and not Type 12, is a target for endocrine therapy of hormone-dependent breast cancer.* Int J Cancer, 2008. **122**(9): p. 1931-40.

68. Ariga, N., et al., *17 beta-Hydroxysteroid dehydrogenase type 1 and type 2 in ductal carcinoma in situ and intraductal proliferative lesions of the human breast.* Anticancer Res, 2000. **20**(2B): p. 1101-8.
69. Miyoshi, Y., et al., *Involvement of up-regulation of 17beta-hydroxysteroid dehydrogenase type 1 in maintenance of intratumoral high estradiol levels in postmenopausal breast cancers.* Int J Cancer, 2001. **94**(5): p. 685-9.
70. Takeyama, J., et al., *17beta-hydroxysteroid dehydrogenase type 1 and 2 expression in the human fetus.* J Clin Endocrinol Metab, 2000. **85**(1): p. 410-6.
71. Gunnarsson, C., et al., *17beta-Hydroxysteroid dehydrogenases involved in local oestrogen synthesis have prognostic significance in breast cancer.* Br J Cancer, 2005. **92**(3): p. 547-52.
72. Vihko, P., et al., *Control of cell proliferation by steroids: the role of 17HSDs.* Mol Cell Endocrinol, 2006. **248**(1-2): p. 141-8.
73. Purohit, A., et al., *The regulation and inhibition of 17beta-hydroxysteroid dehydrogenase in breast cancer.* Mol Cell Endocrinol, 2006. **248**(1-2): p. 199-203.
74. Sasano, H., et al., *New development in intracrinology of breast carcinoma.* Breast Cancer, 2006. **13**(2): p. 129-36.
75. Arispe, N., et al., *beta-Amyloid Ca(2+)-channel hypothesis for neuronal death in Alzheimer disease.* Mol Cell Biochem, 1994. **140**(2): p. 119-25.
76. Davis, R.E., et al., *Mutations in mitochondrial cytochrome c oxidase genes segregate with late-onset Alzheimer disease.* Proc Natl Acad Sci U S A, 1997. **94**(9): p. 4526-31.
77. Beal, M.F., *Mitochondrial dysfunction and oxidative damage in Alzheimer's and Parkinson's diseases and coenzyme Q(10) as a potential treatment.* Journal of Bioenergetics and Biomembranes, 2004. **36**(4): p. 381-386.
78. Du, H., et al., *Synaptic Mitochondrial Pathology in Alzheimer's Disease.* Antioxidants & Redox Signaling, 2012. **16**(12): p. 1467-1475.
79. Leuner, K., et al., *Mitochondrion-Derived Reactive Oxygen Species Lead to Enhanced Amyloid Beta Formation.* Antioxidants & Redox Signaling, 2012. **16**(12): p. 1421-1433.
80. Humphries, K.M., et al., *Inhibition of NADH-linked mitochondrial respiration by 4-hydroxy-2-nonenal.* Biochemistry, 1998. **37**(2): p. 552-7.
81. Blass, J.P., *The mitochondrial spiral. An adequate cause of dementia in the Alzheimer's syndrome.* Ann N Y Acad Sci, 2000. **924**: p. 170-83.
82. Bosetti, F., et al., *Cytochrome c oxidase and mitochondrial F1F0-ATPase (ATP synthase) activities in platelets and brain from patients with Alzheimer's disease.* Neurobiol Aging, 2002. **23**(3): p. 371-6.
83. Lustbader, J.W., et al., *ABAD Directly Links Aß to Mitochondrial Toxicity in Alzheimer's Disease.* Science, 2004. **304**(5669): p. 448-452.
84. Chen, X., et al., *Mitochondrial Abeta: a potential cause of metabolic dysfunction in Alzheimer's disease.* IUBMB Life, 2006. **58**(12): p. 686-94.
85. Takuma, K., et al., *Mitochondrial dysfunction, endoplasmic reticulum stress, and apoptosis in Alzheimer's disease.* J Pharmacol Sci, 2005. **97**(3): p. 312-6.
86. Takuma, K., et al., *ABAD enhances Abeta-induced cell stress via mitochondrial dysfunction.* FASEB J, 2005. **19**(6): p. 597-8.

87. Du Yan, S., et al., *An intracellular protein that binds amyloid-[beta] peptide and mediates neurotoxicity in Alzheimer's disease.* Nature, 1997. **389**(6652): p. 689-695.
88. He, X.Y., et al., *Abundant type 10 17 beta-hydroxysteroid dehydrogenase in the hippocampus of mouse Alzheimer's disease model.* Brain Res Mol Brain Res, 2002. **99**(1): p. 46-53.
89. Torroja, L., et al., *scully, an essential gene of Drosophila, is homologous to mammalian mitochondrial type II L-3-hydroxyacyl-CoA dehydrogenase/amyloid-beta peptide-binding protein.* J Cell Biol, 1998. **141**(4): p. 1009-17.
90. Yan, S.D., et al., *Role of ERAB/L-3-hydroxyacyl-coenzyme A dehydrogenase type II activity in Abeta-induced cytotoxicity.* J Biol Chem, 1999. **274**(4): p. 2145-56.
91. Kissinger, C.R., et al., *Crystal Structure of Human ABAD/HSD10 with a Bound Inhibitor: Implications for Design of Alzheimer's Disease Therapeutics.* Journal of Molecular Biology, 2004. **342**(3): p. 943-952.
92. Du Yan, S., et al., *Amyloid beta -peptide-binding alcohol dehydrogenase is a component of the cellular response to nutritional stress.* J Biol Chem, 2000. **275**(35): p. 27100-9.
93. Yan, S.D., et al., *Mitochondrial dysfunction and Alzheimer's disease: role of amyloid-beta peptide alcohol dehydrogenase (ABAD).* Int J Exp Pathol, 2005. **86**(3): p. 161-71.
94. Yao, J., et al., *Inhibition of amyloid-beta (Abeta) peptide-binding alcohol dehydrogenase-Abeta interaction reduces Abeta accumulation and improves mitochondrial function in a mouse model of Alzheimer's disease.* J Neurosci, 2011. **31**(6): p. 2313-20.
95. Drews, J., *Drug discovery: a historical perspective.* Science, 2000. **287**(5460): p. 1960-4.
96. Engel, P.C., *Enzyme Kinetics (Outline Studies in Biology)*1977, U.S.A: John Wiley & Sons, Inc., New York. p. 45-56.
97. Cornish-Bowden, A., *Fundamentals of Enzyme Kinetics*. Revised Edition ed1995, London: Portland Press Ltd.
98. Cleland, W.W., *The kinetics of enzyme-catalyzed reactions with two or more substrates or products: I. Nomenclature and rate equations.* Biochimica et Biophysica Acta (BBA) - Specialized Section on Enzymological Subjects, 1963. **67**(0): p. 104-137.
99. Purich, D.L., *Contemporary Enzyme Kinetics and Mechanism*. Vol. 20. 2009, USA: Academic Press. p. 279-299, 409.
100. H. John Smith, C.S., *Enzymes and their inhibition: drug development*2004, USA: CRC Press. p. 44-66.
101. Dalziel, K., *Initial Steady State Velocities in the Evaluation of Enzyme-Coenzyme-Substrate Reaction Mechanisms.* Acta Chemica Scandinavica, 1957. **11**(10): p. 1706-1723.
102. Lineweaver, H., et al., *The Determination of Enzyme Dissociation Constants.* Journal of the American Chemical Society, 1934. **56**: p. 658-666.
103. Engel, P.C., *Enzymology*, ed. D.R. B.D. Hames1996, USA and UK: Academic Press, Inc., and BIOS Scientific Publishers Limited. p. 33, 59-65.

104. Cleland, W.W., *The kinetics of enzyme-catalyzed reactions with two or more substrates or products. III. Prediction of initial velocity and inhibition patterns by inspection.* Biochim Biophys Acta, 1963. **67**: p. 188-96.
105. Fromm, H.J., et al., *Kinetic studies of yeast hexokinase.* J Biol Chem, 1962. **237**: p. 3027-32.
106. Sousa, S.F., et al., *Protein-ligand docking: current status and future challenges.* Proteins, 2006. **65**(1): p. 15-26.
107. Kuntz, I.D., et al., *A geometric approach to macromolecule-ligand interactions.* J Mol Biol, 1982. **161**(2): p. 269-88.
108. Kitchen, D.B., et al., *Docking and scoring in virtual screening for drug discovery: methods and applications.* Nat Rev Drug Discov, 2004. **3**(11): p. 935-49.
109. Ha, S., et al., *Evaluation of docking/scoring approaches: a comparative study based on MMP3 inhibitors.* J Comput Aided Mol Des, 2000. **14**(5): p. 435-48.
110. Teague, S.J., *Implications of protein flexibility for drug discovery.* Nat Rev Drug Discov, 2003. **2**(7): p. 527-41.
111. Carlson, H.A., *Protein flexibility and drug design: how to hit a moving target.* Curr Opin Chem Biol, 2002. **6**(4): p. 447-52.
112. Carlson, H.A., *Protein flexibility is an important component of structure-based drug discovery.* Curr Pharm Des, 2002. **8**(17): p. 1571-8.
113. Gohlke, H., et al., *Knowledge-based scoring function to predict protein-ligand interactions.* J Mol Biol, 2000. **295**(2): p. 337-56.
114. R.Leach, A., *Molecular Modelling-principles and applications.* Second ed2001: Pearson Education Ltd. 744.
115. Eldridge, M.D., et al., *Empirical scoring functions: I. The development of a fast empirical scoring function to estimate the binding affinity of ligands in receptor complexes.* J Comput Aided Mol Des, 1997. **11**(5): p. 425-45.
116. Annamala, M.K., et al., *Docking of phosphonate and trehalose analog inhibitors into M. tuberculosis mycolyltransferase Ag85C: Comparison of the two scoring fitness functions GoldScore and ChemScore, in the GOLD software.* Bioinformation, 2007. **1**(9): p. 339-50.
117. Jorgensen, W.L., et al., *Development and testing of the OPLS all-atom force field on conformational energetics and properties of organic liquids.* Journal of the American Chemical Society, 1996. **118**(45): p. 11225-11236.
118. Jorgensen, W.L., et al., *Development of the OPLS-AA force field for organic and biomolecular systems.* Abstracts of Papers of the American Chemical Society, 1998. **216**: p. U696-U696.
119. Friesner, R.A., et al., *Extra precision glide: docking and scoring incorporating a model of hydrophobic enclosure for protein-ligand complexes.* J Med Chem, 2006. **49**(21): p. 6177-96.
120. Jorgensen, W.L., et al., *Development and Testing of the OPLS All-Atom Force Field on Conformational Energetics and Properties of Organic Liquids.* Journal of the American Chemical Society, 1996. **118**(45): p. 11225-11236.
121. Gibson, K.D., et al., *Minimization of Polypeptide Energy, Vi. Systematic Searches for Low-Energy Conformations of Deca-L-Alanine and the Octapeptide Loop of Ribonuclease.* Proc Natl Acad Sci U S A, 1969. **63**(1): p. 9-15.

122. Gibson, K.D., et al., *Minimization of polypeptide energy. I. Preliminary structures of bovine pancreatic ribonuclease S-peptide.* Proc Natl Acad Sci U S A, 1967. **58**(2): p. 420-7.
123. Nakamura, S., et al., *New method for parallel computation of Hessian matrix of conformational energy function in internal coordinates.* J Comput Chem, 2002. **23**(4): p. 463-9.
124. Bouzida, D., et al., *Efficient Monte Carlo methods for the computer simulation of biological molecules.* Phys Rev A, 1992. **45**(12): p. 8894-8901.
125. Metropolis, N., et al., *Equation of State Calculations by Fast Computing Machines.* Journal of Chemical Physics, 1953. **21**(6): p. 1087-1092.
126. Wainwright, B.J.A.a.T.E., *Phase Transition for a Hard Sphere System.* J. Chem. Phys, 1957. **27**(November 1957): p. 1208.
127. Wainwright, B.J.A.a.T.E., *Studies in Molecular Dynamics. I. General Method.* J. Chem. Phys, 1959. **31**(August 1959): p. 459.
128. Rahman, A., *Correlations in Motion of Atoms in Liquid Argon.* Physical Review a-General Physics, 1964. **136**(2A): p. A405-&.
129. Stillinger, F.H., et al., *Molecular dynamics study of liquid water under high compression.* J. Chem. Phys, 1974. **61**: p. 4973
130. McCammon, J.A., et al., *Dynamics of folded proteins.* Nature, 1977. **267**(5612): p. 585-90.
131. Daura, X., et al., *Reversible peptide folding in solution by molecular dynamics simulation.* J Mol Biol, 1998. **280**(5): p. 925-32.
132. Daura, X., *Molecular dynamics simulation of peptide folding.* Theoretical Chemistry Accounts, 2006. **116**(1-3): p. 297-306.
133. Gao, J.L., et al., *Quantum mechanical methods for enzyme kinetics.* Annual Review of Physical Chemistry, 2002. **53**: p. 467-505.
134. Warshel, A., et al., *Theoretical studies of enzymic reactions: dielectric, electrostatic and steric stabilization of the carbonium ion in the reaction of lysozyme.* J Mol Biol, 1976. **103**(2): p. 227-49.
135. Field, M.J., et al., *A Combined Quantum-Mechanical and Molecular Mechanical Potential for Molecular-Dynamics Simulations.* Journal of Computational Chemistry, 1990. **11**(6): p. 700-733.
136. Gao, J.L., *Hybrid quantum and molecular mechanical simulations: An alternative avenue to solvent effects in organic chemistry.* Accounts of Chemical Research, 1996. **29**(6): p. 298-305.
137. Cunningham, M.A., et al., *Simulation of the enzyme reaction mechanism of malate dehydrogenase.* Biochemistry, 1997. **36**(16): p. 4800-4816.
138. Jiali Gao, M.A.T., *Combined Quantum Mechanical and Molecular Mechanical Methods*. ACS Symposium Series. Vol. 712. 1998: American Chemical Society. 324.
139. Stanton, R.V., et al., *Development and Application of Quantum-Mechanical Molecular Mechanical Coupled Potentials.* Abstracts of Papers of the American Chemical Society, 1994. **207**: p. 19-Comp.
140. Murphy, R.B., et al., *Frozen orbital QM/MM methods for density functional theory.* Chemical Physics Letters, 2000. **321**(1-2): p. 113-120.

141. Wang, S., et al., *Ab Initio Quantum Mechanical/Molecular Mechanical Molecular Dynamics Simulation of Enzyme Catalysis: The Case of Histone Lysine Methyltransferase SET7/9.* The Journal of Physical Chemistry B, 2007. **111**(14): p. 3758-3764.
142. Lin, P., et al., *Searching for the minimum energy path in the sulfuryl transfer reaction catalyzed by human estrogen sulfotransferase: Role of enzyme dynamics.* International Journal of Quantum Chemistry, 2006. **106**(14): p. 2981-2998.
143. Bergès, J., et al., *QM/MM study of electron addition on protein disulfide bonds.* Chemical Physics Letters, 2006. **421**(1–3): p. 63-67.
144. Hu, P., et al., *Catalytic Mechanism and Product Specificity of the Histone Lysine Methyltransferase SET7/9: An ab Initio QM/MM-FE Study with Multiple Initial Structures.* Journal of the American Chemical Society, 2006. **128**(4): p. 1272-1278.
145. Zhang, X., et al., *A Quantum Mechanics/Molecular Mechanics Study of the Catalytic Mechanism and Product Specificity of Viral Histone Lysine Methyltransferase†.* Biochemistry, 2007. **46**(34): p. 9743-9751.
146. Puig, E., et al., *On the Ionization State of the Substrate in the Active Site of Glutamate Racemase. A QM/MM Study about the Importance of Being Zwitterionic†.* The Journal of Physical Chemistry A, 2005. **110**(2): p. 717-725.
147. Major, D.T., et al., *Transition State Stabilization and α-Amino Carbon Acidity in Alanine Racemase.* Journal of the American Chemical Society, 2006. **128**(25): p. 8114-8115.
148. Dybala-Defratyka, A., et al., *Coupling of hydrogenic tunneling to active-site motion in the hydrogen radical transfer catalyzed by a coenzyme B12-dependent mutase.* Proc Natl Acad Sci U S A, 2007. **104**(26): p. 10774-9.
149. Ma, S., et al., *Molecular Dynamics Simulations of the Catalytic Pathway of a Cysteine Protease: A Combined QM/MM Study of Human Cathepsin K.* Journal of the American Chemical Society, 2007. **129**(44): p. 13633-13645.
150. Kästner, J., et al., *QM/MM Free-Energy Perturbation Compared to Thermodynamic Integration and Umbrella Sampling: Application to an Enzymatic Reaction.* Journal of Chemical Theory and Computation, 2006. **2**(2): p. 452-461.
151. Carvalho, A.T.P., et al., *Determination of the ΔpKa between the active site cysteines of thioredoxin and DsbA.* Journal of Computational Chemistry, 2006. **27**(8): p. 966-975.
152. Nunthaboot, N., et al., *Hybrid Quantum Mechanical/Molecular Mechanical Molecular Dynamics Simulations of HIV-1 Integrase/Inhibitor Complexes.* Biophysical Journal, 2007. **93**(10): p. 3613-3626.
153. Pieraccini, S., et al., *Modeling enzymatic processes: A molecular simulation analysis of the origins of regioselectivity.* Chemical Physics Letters, 2006. **418**(4–6): p. 373-376.
154. Elstner, M., et al., *A self-consistent charge density-functional based tight-binding scheme for large biomolecules.* Physica Status Solidi B-Basic Research, 2000. **217**(1): p. 357-376.

155. Frauenheim, T., et al., *A self-consistent charge density-functional based tight-binding method for predictive materials simulations in physics, chemistry and biology.* Physica Status Solidi B-Basic Research, 2000. **217**(1): p. 41-62.
156. Elstner, M., et al., *Self consistent-charge density-functional tight-binding method for simulations of biological molecules.* Multiscale Modelling of Materials, 1999. **538**: p. 541-546.
157. Elstner, M., et al., *Self-consistent-charge density-functional tight-binding method for simulations of complex materials properties.* Physical Review B, 1998. **58**(11): p. 7260-7268.
158. Sreerama, N., et al., *Theoretical-Study of the Crystal-Field Effects on the Transition Dipole-Moments in Methylated Adenines.* Journal of Physical Chemistry, 1994. **98**(41): p. 10397-10407.
159. Callis, P.R., et al., *Short range photoinduced electron transfer in proteins: QM-MM simulations of tryptophan and flavin fluorescence quenching in proteins.* Chemical Physics, 2006. **326**(1): p. 230-239.
160. Nakatani, N., et al., *Red light in chemiluminescence and yellow-green light in bioluminescence: color-tuning mechanism of firefly, Photinus pyralis, studied by the symmetry-adapted cluster-configuration interaction method.* J Am Chem Soc, 2007. **129**(28): p. 8756-65.
161. Fujimoto, K., et al., *Theoretical studies on the color-tuning mechanism in retinal proteins.* Journal of Chemical Theory and Computation, 2007. **3**(2): p. 605-618.
162. Fujimoto, K., et al., *On the color-tuning mechanism of Human-Blue visual pigment: SAC-CI and QM/MM study.* Chemical Physics Letters, 2006. **432**(1-3): p. 252-256.
163. Patnaik, S.S., et al., *Computational study of the absorption spectra of green fluorescent protein mutants.* Biopolymers, 2007. **85**(3): p. 253-263.
164. Grigorenko, B., et al., *Ground-State Structures and Vertical Excitations for the Kindling Fluorescent Protein asFP595.* The Journal of Physical Chemistry B, 2006. **110**(37): p. 18635-18640.
165. Grigorenko, B., et al., *trans and cis Chromophore structures in the kindling fluorescent protein asFP595.* Chemical Physics Letters, 2006. **424**(1–3): p. 184-188.
166. Nemukhin, A.V., et al., *Modeling dioxygen binding to the non-heme iron-containing enzymes.* International Journal of Quantum Chemistry, 2006. **106**(10): p. 2184-2190.
167. Sugihara, M., et al., *Origin and consequences of steric strain in the rhodopsin binding pocket.* Biochemistry, 2006. **45**(3): p. 801-810.
168. Bravaya, K., et al., *An opsin shift in rhodopsin: Retinal S0-S1 excitation in protein, in solution, and in the gas phase.* Journal of the American Chemical Society, 2007. **129**(43): p. 13035-13042.
169. Hoffmann, M., et al., *Color tuning in rhodopsins: The mechanism for the spectral shift between bacteriorhodopsin and sensory rhodopsin II.* Journal of the American Chemical Society, 2006. **128**(33): p. 10808-10818.
170. Singh, U.C., et al., *A Combined Abinitio Quantum-Mechanical and Molecular Mechanical Method for Carrying out Simulations on Complex Molecular-Systems*

- *Applications to the Ch3cl + Cl- Exchange-Reaction and Gas-Phase Protonation of Polyethers.* Journal of Computational Chemistry, 1986. **7**(6): p. 718-730.
171. Antes, I., et al., *Adjusted Connection Atoms for Combined Quantum Mechanical and Molecular Mechanical Methods.* The Journal of Physical Chemistry A, 1999. **103**(46): p. 9290-9295.
172. Zhang, Y.K., et al., *A pseudobond approach to combining quantum mechanical and molecular mechanical methods.* Journal of Chemical Physics, 1999. **110**(1): p. 46-54.
173. Zhang, Y.K., *Improved pseudobonds for combined ab initio quantum mechanical/molecular mechanical methods.* Journal of Chemical Physics, 2005. **122**(2).
174. Zhang, Y., *Pseudobond ab initio QM/MM approach and its applications to enzyme reactions.* Theoretical Chemistry Accounts: Theory, Computation, and Modeling (Theoretica Chimica Acta), 2006. **116**(1): p. 43-50.
175. Laio, A., et al., *A Hamiltonian electrostatic coupling scheme for hybrid Car-Parrinello molecular dynamics simulations.* Journal of Chemical Physics, 2002. **116**(16): p. 6941-6947.
176. Cornell, W.D., et al., *A Second Generation Force Field for the Simulation of Proteins, Nucleic Acids, and Organic Molecules.* Journal of the American Chemical Society, 1995. **117**(19): p. 5179-5197.
177. Wang, J., et al., *How well does a restrained electrostatic potential (RESP) model perform in calculating conformational energies of organic and biological molecules?* Journal of Computational Chemistry, 2000. **21**(12): p. 1049-1074.
178. Duan, Y., et al., *A point-charge force field for molecular mechanics simulations of proteins based on condensed-phase quantum mechanical calculations.* Journal of Computational Chemistry, 2003. **24**(16): p. 1999-2012.
179. MacKerell, A.D., et al., *All-Atom Empirical Potential for Molecular Modeling and Dynamics Studies of Proteins†.* The Journal of Physical Chemistry B, 1998. **102**(18): p. 3586-3616.
180. Foloppe, N., et al., *All-atom empirical force field for nucleic acids: I. Parameter optimization based on small molecule and condensed phase macromolecular target data.* Journal of Computational Chemistry, 2000. **21**(2): p. 86-104.
181. MacKerell, A.D., et al., *All-atom empirical force field for nucleic acids: II. Application to molecular dynamics simulations of DNA and RNA in solution.* Journal of Computational Chemistry, 2000. **21**(2): p. 105-120.
182. Kaminski, G.A., et al., *Evaluation and Reparametrization of the OPLS-AA Force Field for Proteins via Comparison with Accurate Quantum Chemical Calculations on Peptides†.* The Journal of Physical Chemistry B, 2001. **105**(28): p. 6474-6487.
183. Scott, W.R.P., et al., *The GROMOS Biomolecular Simulation Program Package.* The Journal of Physical Chemistry A, 1999. **103**(19): p. 3596-3607.
184. Sousa, S.F., et al., *Theoretical studies on farnesyl transferase: Evidence for thioether product coordination to the active-site zinc sphere.* Journal of Computational Chemistry, 2007. **28**(7): p. 1160-1168.
185. Saen-oon, S., et al., *Insight into analysis of interactions of saquinavir with HIV-1 protease in comparison between the wild-type and G48V and G48V/L90M*

mutants based on QM and QM/MM calculations. Journal of Molecular Graphics and Modelling, 2007. **26**(4): p. 720-727.
186. Sinnecker, S., et al., *Protein-cofactor interactions in bacterial reaction centers from Rhodobacter sphaeroides R-26: Effect of hydrogen bonding on the electronic and geometric structure of the primary quinone. A density functional theory study.* Physical Chemistry Chemical Physics, 2006. **8**(48): p. 5659-5670.
187. Robertazzi, A., et al., *Gas-Phase DNA Oligonucleotide Structures. A QM/MM and Atoms in Molecules Study.* The Journal of Physical Chemistry A, 2006. **110**(11): p. 3992-4000.
188. Maseras, F., et al., *Imomm - a New Integrated Ab-Initio Plus Molecular Mechanics Geometry Optimization Scheme of Equilibrium Structures and Transition-States.* Journal of Computational Chemistry, 1995. **16**(9): p. 1170-1179.
189. Claeyssens, F., et al., *High-Accuracy Computation of Reaction Barriers in Enzymes.* Angewandte Chemie, 2006. **118**(41): p. 7010-7013.
190. Shaik, S., et al., *Theoretical perspective on the structure and mechanism of cytochrome P450 enzymes.* Chemical Reviews, 2005. **105**(6): p. 2279-2328.
191. Walker, R.C., et al., *Comparison of basis set effects and the performance of ab initio and DFT methods for probing equilibrium fluctuations.* Journal of Computational Chemistry, 2007. **28**(2): p. 478-490.
192. Wymore, T., et al., *Mechanistic Implications of the Cysteine−Nicotinamide Adduct in Aldehyde Dehydrogenase Based on Quantum Mechanical/Molecular Mechanical Simulations†.* Biochemistry, 2007. **46**(33): p. 9495-9506.
193. Harvey, J.N., et al., *QM/MM modeling of compound I active species in cytochrome P450, cytochrome C peroxidase, and ascorbate peroxidase.* Journal of Computational Chemistry, 2006. **27**(12): p. 1352-1362.
194. Ranaghan , K.E., et al., *Analysis of Classical and Quantum Paths for Deprotonation of Methylamine by Methylamine Dehydrogenase.* ChemPhysChem, 2007. **8**(12): p. 1816-1835.
195. Masgrau, L., et al., *Atomic description of an enzyme reaction dominated by proton tunneling.* Science, 2006. **312**(5771): p. 237-41.
196. Masgrau, L., et al., *Tunneling and Classical Paths for Proton Transfer in an Enzyme Reaction Dominated by Tunneling: Oxidation of Tryptamine by Aromatic Amine Dehydrogenase.* The Journal of Physical Chemistry B, 2007. **111**(11): p. 3032-3047.
197. Amara, P., et al., *Carbon Monoxide Dehydrogenase Reaction Mechanism: A Likely Case of Abnormal CO2 Insertion to a Ni-H- Bond.* Inorg Chem, 2011. **50**(5): p. 1868-1878.
198. Bochevarov, A.D., et al., *Insights into the Different Dioxygen Activation Pathways of Methane and Toluene Monooxygenase Hydroxylases.* Journal of the American Chemical Society, 2011. **133**(19): p. 7384-7397.
199. Zhang, X., et al., *Mechanism of methanol oxidation by quinoprotein methanol dehydrogenase.* Proc Natl Acad Sci U S A, 2007. **104**(3): p. 745-9.
200. Alzate-Morales, J.H., et al., *A Computational Study of the Protein-Ligand Interactions in CDK2 Inhibitors: Using Quantum Mechanics/Molecular*

Mechanics Interaction Energy as a Predictor of the Biological Activity. Biophysical Journal, 2007. **92**(2): p. 430-439.
201. Wang, L., et al., *A Water-Mediated and Substrate-Assisted Catalytic Mechanism for Sulfolobus solfataricus DNA Polymerase IV.* Journal of the American Chemical Society, 2007. **129**(15): p. 4731-4737.
202. Rod, T.H., et al., *Implicit versus explicit solvent in free energy calculations of enzyme catalysis: Methyl transfer catalyzed by catechol O-methyltransferase.* Journal of Chemical Physics, 2006. **124**(17).
203. Blumberger, J., et al., *Peptide Hydrolysis in Thermolysin: Ab Initio QM/MM Investigation of the Glu143-Assisted Water Addition Mechanism.* Journal of Chemical Theory and Computation, 2007. **3**(5): p. 1837-1850.
204. Ishida, T., *Low-Barrier Hydrogen Bond Hypothesis in the Catalytic Triad Residue of Serine Proteases: Correlation between Structural Rearrangement and Chemical Shifts in the Acylation Process†.* Biochemistry, 2006. **45**(17): p. 5413-5420.
205. Cheng, Y., et al., *Acetylcholinesterase: Mechanisms of Covalent Inhibition of Wild-Type and H447I Mutant Determined by Computational Analyses.* Journal of the American Chemical Society, 2007. **129**(20): p. 6562-6570.
206. Riccardi, D., et al., *"Proton Holes" in Long-Range Proton Transfer Reactions in Solution and Enzymes: A Theoretical Analysis.* Journal of the American Chemical Society, 2006. **128**(50): p. 16302-16311.
207. Kamachi, T., et al., *Computational Mutation Analysis of Hydrogen Abstraction and Radical Rearrangement Steps in the Catalysis of Coenzyme B12-Dependent Diol Dehydratase.* Chemistry – A European Journal, 2007. **13**(28): p. 7864-7873.
208. van der Kamp, M.W., et al., *Substrate polarization in enzyme catalysis: QM/MM analysis of the effect of oxaloacetate polarization on acetyl-CoA enolization in citrate synthase.* Proteins: Structure, Function, and Bioinformatics, 2007. **69**(3): p. 521-535.
209. Hanoian, P., et al., *Water in the active site of ketosteroid isomerase.* Biochemistry, 2011. **50**(31): p. 6689-700.
210. Cisneros, G.A., et al., *Theoretical and Experimental Determination on Two Substrates Turned over by 4-Oxalocrotonate Tautomerase†.* The Journal of Physical Chemistry A, 2005. **110**(2): p. 700-708.
211. Szefczyk, B., et al., *Quantum chemical analysis of reaction paths in chorismate mutase: Conformational effects and electrostatic stabilization.* International Journal of Quantum Chemistry, 2007. **107**(12): p. 2274-2285.
212. Ruiz-Pernía, J.J., et al., *Hybrid Quantum Mechanics/Molecular Mechanics Simulations with Two-Dimensional Interpolated Corrections: Application to Enzymatic Processes.* The Journal of Physical Chemistry B, 2006. **110**(35): p. 17663-17670.
213. Ishida, T., et al., *All Electron Quantum Chemical Calculation of the Entire Enzyme System Confirms a Collective Catalytic Device in the Chorismate Mutase Reaction.* The Journal of Physical Chemistry B, 2005. **110**(3): p. 1457-1463.
214. Dybala-Defratyka, A., et al., *Coupling of hydrogenic tunneling to active-site motion in the hydrogen radical transfer catalyzed by a coenzyme B-12-dependent*

mutase. Proceedings of the National Academy of Sciences of the United States of America, 2007. **104**(26): p. 10774-10779.
215. Bondar, A.-N., et al., *Structural and energetic determinants of primary proton transfer in bacteriorhodopsin.* Photochemical & Photobiological Sciences, 2006. **5**(6): p. 547-552.
216. Sato, Y., et al., *Computational Analysis of the Proton Translocation from Asp96 to Schiff Base in Bacteriorhodopsin.* The Journal of Physical Chemistry B, 2006. **110**(45): p. 22804-22812.
217. Kamiya, M., et al., *Proton Transfer and Associated Molecular Rearrangements in the Photocycle of Photoactive Yellow Protein: Role of Water Molecular Migration on the Proton Transfer Reaction.* The Journal of Physical Chemistry B, 2007. **111**(11): p. 2948-2956.
218. Sugihara, M., et al., *Origin and Consequences of Steric Strain in the Rhodopsin Binding Pocket†.* Biochemistry, 2005. **45**(3): p. 801-810.
219. Gascón, J.A., et al., *Computational Studies of the Primary Phototransduction Event in Visual Rhodopsin.* Accounts of Chemical Research, 2006. **39**(3): p. 184-193.
220. Woiczikowski, P.B., et al., *Nonadiabatic QM/MM Simulations of Fast Charge Transfer in Escherichia coli DNA Photolyase.* The Journal of Physical Chemistry B, 2011. **115**(32): p. 9846-9863.
221. Garrec, J., et al., *Insights into Intrastrand Cross-Link Lesions of DNA from QM/MM Molecular Dynamics Simulations.* Journal of the American Chemical Society, 2011. **134**(4): p. 2111-2119.
222. Futera, Z., et al., *Binding of piano-stool Ru(II) complexes to DNA; QM/MM study.* Journal of Computational Chemistry, 2012: p. n/a-n/a.
223. Sundaresan, N., et al., *Role of Mg2+ and Ca2+ in DNA Bending: Evidence from an ONIOM-Based QM-MM Study of a DNA Fragment.* The Journal of Physical Chemistry A, 2006. **110**(28): p. 8826-8831.
224. Rogacheva, M.V., et al., *Impact of Pyrophosphate and O-Ethyl-Substituted Pyrophosphate Groups on DNA Structure.* The Journal of Physical Chemistry B, 2006. **111**(2): p. 432-438.
225. Robertazzi, A., et al., *A QM/MM Study of Cisplatin–DNA Oligonucleotides: From Simple Models to Realistic Systems.* Chemistry – A European Journal, 2006. **12**(22): p. 5747-5756.
226. Magistrato, A., et al., *Binding of Novel Azole-Bridged Dinuclear Platinum(II) Anticancer Drugs to DNA: Insights from Hybrid QM/MM Molecular Dynamics Simulations†.* The Journal of Physical Chemistry B, 2005. **110**(8): p. 3604-3613.
227. Spiegel, K., et al., *Duocarmycins Binding to DNA Investigated by Molecular Simulation†.* The Journal of Physical Chemistry B, 2006. **110**(8): p. 3647-3660.
228. Vargiu, A.V., et al., *Anthramycin−DNA Binding Explored by Molecular Simulations.* The Journal of Physical Chemistry B, 2006. **110**(48): p. 24687-24695.
229. Tuttle, T., et al., *A QM/MM Study of the Bergman Reaction of Dynemicin A in the Minor Groove of DNA.* The Journal of Physical Chemistry B, 2007. **111**(28): p. 8321-8328.

230. Gani, O.A.B.S.M., et al., *Theoretical calculations of the catalytic triad in short-chain alcohol dehydrogenases/reductases.* Biophysical Journal, 2008. **94**(4): p. 1412-1427.
231. Chen, Z., et al., *Site-directed mutagenesis of glycine-14 and two "critical" cysteinyl residues in Drosophila alcohol dehydrogenase.* Biochemistry, 1990. **29**(5): p. 1112-8.
232. Chen, Z., et al., *Role of aspartic acid 38 in the cofactor specificity of Drosophila alcohol dehydrogenase.* Eur J Biochem, 1991. **202**(2): p. 263-7.
233. Albalat, R., et al., *Drosophila lebanonensis ADH: analysis of recombinant wild-type enzyme and site-directed mutants. The effect of restoring the consensus sequence in two positions.* FEBS Lett, 1994. **341**(2-3): p. 171-6.
234. Chen, Z., et al., *Adding a positive charge at residue 46 of Drosophila alcohol dehydrogenase increases cofactor specificity for NADP+*. FEBS Lett, 1994. **356**(1): p. 81-5.
235. Albalat, R., et al., *Involvement of the C-terminal tail in the activity of Drosophila alcohol dehydrogenase. Evaluation of truncated proteins constructed by site-directed mutagenesis.* Eur J Biochem, 1995. **233**(2): p. 498-505.
236. Ribas de Pouplana, L., et al., *The active site architecture of a short-chain dehydrogenase defined by site-directed mutagenesis and structure modeling.* Biochemistry, 1994. **33**(23): p. 7047-55.
237. Dalziel, K., *Initial steady state velocities in the evaluation on enzyme-coenzyme-substrate reactions.* Acta Chem Scand, 1957. **11**: p. 1706 - 1723.
238. Theorell, H., et al., *Liver Alcohol Dehydrogenase-Dpn-Pyrazole Complex: A Model of a Ternary Intermediate in the Enzyme Reaction.* Biochem Z, 1963. **338**: p. 537-53.
239. Winberg, J.O., et al., *Alcohol dehydrogenase from the fruitfly Drosophila melanogaster. Inhibition studies of the alleloenzymes AdhS and AdhUF.* Biochim Biophys Acta, 1982. **704**(1): p. 17-25.
240. Winberg, J.O., et al., *The alcohol dehydrogenase alleloenzymes AdhS and AdhF from the fruitfly Drosophila melanogaster: an enzymatic rate assay to determine the active-site concentration.* Biochem Genet, 1985. **23**(3-4): p. 205-16.
241. Schrödinger, *Maestro, version 9.2, Schrödinger, LLC, New York, NY, 2011.*, 2011.
242. Maestro, v., Schrödinger, LLC, New York, NY, 2010.
243. Epik, v., Schrödinger, LLC, New York, NY, 2011.
244. Glide, v., Schrödinger, LLC, New York, NY, 2011.
245. Desmond Molecular Dynamics System, v., D. E. Shaw Research, New York, NY, 2011.
246. Martyna, G.J., et al., *Nose-Hoover Chains - the Canonical Ensemble Via Continuous Dynamics.* Journal of Chemical Physics, 1992. **97**(4): p. 2635-2643.
247. Martyna, G.J., et al., *Constant-Pressure Molecular-Dynamics Algorithms.* Journal of Chemical Physics, 1994. **101**(5): p. 4177-4189.
248. Essmann, U., et al., *A Smooth Particle Mesh Ewald Method.* Journal of Chemical Physics, 1995. **103**(19): p. 8577-8593.
249. Murphy, R.B., et al., *A mixed quantum mechanics/molecular mechanics (QM/MM) method for large-scale modeling of chemistry in protein environments.* Journal of Computational Chemistry, 2000. **21**(16): p. 1442-1457.

250. Philipp, D.M., et al., *Mixed ab initio QM/MM modeling using frozen orbitals and tests with alanine dipeptide and tetrapeptide.* Journal of Computational Chemistry, 1999. **20**(14): p. 1468-1494.
251. Becke, A.D., *A New Mixing of Hartree-Fock and Local Density-Functional Theories.* Journal of Chemical Physics, 1993. **98**(2): p. 1372-1377.
252. Jorgensen, J.H., et al., *Development of interpretive criteria and quality control limits for macrolide and clindamycin susceptibility testing of Streptococcus pneumoniae.* J Clin Microbiol, 1996. **34**(11): p. 2679-84.
253. QSite, v., Schrödinger, LLC, New York, NY, 2011.
254. Engel, T., *Quantum Chemistry and Spectroscopy*2012, USA: Pearson Education, Inc. 507.
255. Kallberg, Y., et al., *Short-chain dehydrogenase/reductase (SDR) relationships: a large family with eight clusters common to human, animal, and plant genomes.* Protein Sci, 2002. **11**(3): p. 636-41.
256. Kavanagh, K., et al., *The SDR superfamily: functional and structural diversity within a family of metabolic and regulatory enzymes.* Cellular and Molecular Life Sciences, 2008. **65**(24): p. 3895-3906.
257. Bray, J.E., et al., *The human short-chain dehydrogenase/reductase (SDR) superfamily: A bioinformatics summary.* Chemico-Biological Interactions, 2009. **178**(1-3): p. 99-109.
258. Hovik, R., et al., *Drosophila melanogaster alcohol dehydrogenase: substrate specificity of the ADHF alleloenzyme.* Insect Biochem, 1984. **14**: p. 345 - 351.
259. Winberg, J.O., et al., *Drosophila alcohol dehydrogenase: stereoselective hydrogen transfer from ethanol.* Biochem Mol Biol Int, 1993. **31**(4): p. 651-8.
260. Yimingjiang Wuxiuer., et al., *An Intact Eight-Membered Water Chain in Short Chain Dehydrogenases/Reductases is Essential for Enzyme Activity.* Febs Journal, in press, 2012.

Paper 1

Paper 2

Paper 3

ISBN xxx-xx-xxxx-xxx-x